Molecular Therapy
Original Article

Exosome-Mediated miR-155 Transfer from Smooth Muscle Cells to Endothelial Cells Induces Endothelial Injury and Promotes Atherosclerosis

Bin Zheng,[1,5] Wei-na Yin,[1,2,5] Toru Suzuki,[3] Xin-hua Zhang,[1] Yu Zhang,[1] Li-li Song,[1] Li-shuang Jin,[1] Hong Zhan,[4] Hong Zhang,[1] Jin-shui Li,[1] and Jin-kun Wen[1]

[1]Department of Biochemistry and Molecular Biology, Key Laboratory of Neural and Vascular Biology, Ministry of Education, Hebei Medical University, Shijiazhuang 050017, China; [2]Paediatric Department, Handan First Hospital, Handan 056000, China; [3]Department of Cardiovascular Sciences and NIHR Leicester Cardiovascular Biomedical Research Unit, Glenfield Hospital, Groby Road, Leicester LE3 9QP, UK; [4]Department of Cardiovascular Sciences, Jichi Medical University, 3311-1 Yakushiji, Shimotsuke-shi, Tochigi-ken 329-0498, Japan

The vascular response to pro-atherosclerotic factors is a multifactorial process involving endothelial cells (ECs), macrophages (MACs), and smooth muscle cells (SMCs), although the mechanism by which these cell types communicate with each other in response to environmental cues is yet to be understood. Here, we show that miR-155, which is significantly expressed and secreted in Krüppel-like factor 5 (KLF5)-overexpressing vascular smooth muscle cells (VSMCs), is a potent regulator of endothelium barrier function through regulating endothelial targeting tight junction protein expression. VSMCs-derived exosomes mediate the transfer of KLF5-induced miR-155 from SMCs to ECs, which, in turn, destroys tight junctions and the integrity of endothelial barriers, leading to an increased endothelial permeability and enhanced atherosclerotic progression. Moreover, overexpression of miR-155 in ECs inhibits endothelial cell proliferation/migration and re-endothelialization in vitro and in vivo and thus increases vascular endothelial permeability. Blockage of the exosome-mediated transfer of miR-155 between these two cells may serve as a therapeutic target for atherosclerosis.

INTRODUCTION

Atherosclerosis, the underlying cause of myocardial infarction and stroke, is a chronic progressive inflammatory disease and the leading cause of death worldwide.[1] It is well known that endothelial cells (ECs), macrophages, and smooth muscle cells (SMCs) participate in atherogenesis.[2] During the development of atherosclerosis, ECs are exposed to various damaging stimuli (such as oxLDL), which trigger vascular endothelial injury. Vascular smooth muscle cell (VSMC) activation and macrophage invasion promote the formation of atherosclerotic plaque. Therefore, the effective prevention and treatment of atherosclerosis should improve vascular endothelial function as well as inhibit VSMCs and macrophage activation.[2]

Krüppel-like factor 5 (KLF5), a zinc-finger-containing transcription factor, plays a central role in cardiovascular remodeling by mediating SMC proliferation and migration, both of which are essential to atherosclerotic plaque formation.[3,4] Interestingly, our preliminary study found that KLF5$^{Tgln-/-}$apoE$^{-/-}$ mice (a VSMC-specific KLF5-knockout strain) exhibited significant inhibition of VSMC proliferation and relative normal endothelial function (Figure 1), indicating an important physiological link between SMC-expressed KLF5 and ECs during atherogenesis. These prompted us to investigate whether KLF5-mediated communication between ECs and SMCs is involved in the development of atherosclerosis. However, it remains to be clarified how the KLF5 that is expressed in SMCs exerts regulatory effects on endothelial function.

MicroRNAs (miRNAs) have been observed in secreted exosomes, which range from 30 to 100 nm in size and are composed of RNAs, miRNAs, and soluble and membrane proteins.[5] Many cells can secrete miRNAs via exosomes, and these exosomal miRNAs exert their regulatory effects on recipient cells, which suggests that the exosomal transfer of miRNAs could be a novel mechanism for intercellular communication.[6,7] Therefore, we hypothesize that KLF5 expressed in VSMCs regulates endothelial function through exosomal miRNAs. Despite significant progress in our understanding of how miRNAs influence atherosclerotic plaque formation in vivo, many aspects of their regulation and function remain unclear.

Received 5 September 2016; accepted 23 March 2017;
http://dx.doi.org/10.1016/j.ymthe.2017.03.031.

[5]These authors contributed equally to this work

Correspondence: Jin-kun Wen, Department of Biochemistry and Molecular Biology, Key Laboratory of Neural and Vascular Biology, Ministry of Education, Hebei Medical University, No. 361 Zhongshan East Road, Shijiazhuang 050017, China.
E-mail: wjk@hebmu.edu.cn
Correspondence: Bin Zheng, Department of Biochemistry and Molecular Biology, Key Laboratory of Neural and Vascular Biology, Ministry of Education, Hebei Medical University, No. 361 Zhongshan East Road, Shijiazhuang 050017, China.
E-mail: doublezb@hebmu.edu.cn

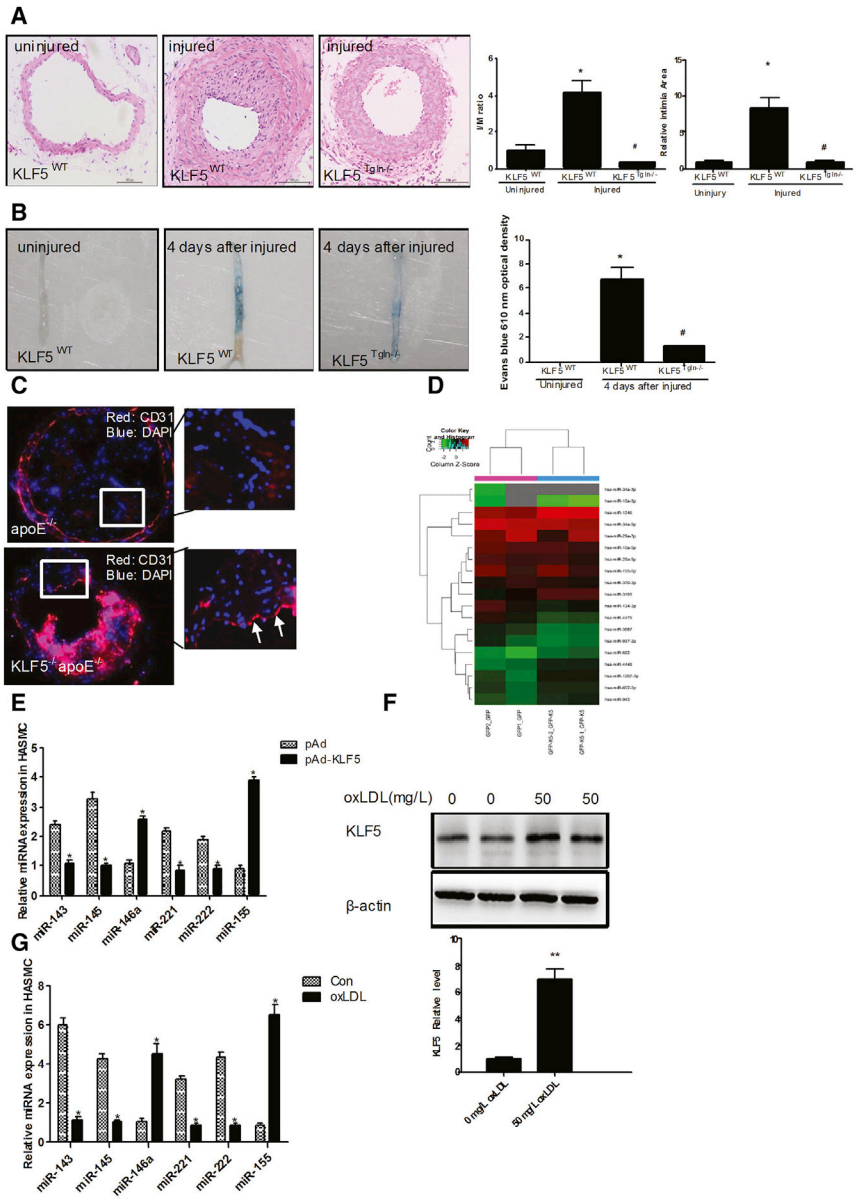

Figure 1. KLF5 Regulates Expression of miRNAs, Particularly miR-155

(A) Neointima hyperplasia was determined on H&E-stained cross sections of wire-injured femoral arteries 14 days after injury in KLF5$^{Tgln-/-}$ mice or KLF5^{wt} mice. (n = 6 each group). Scale bar, 100 μm. *p < 0.05 versus KLF5^{wt} mice (uninjured). #p < 0.05 versus KLF5^{wt} mice (injured). (B) The extent of re-endothelialization was evaluated in Evans-blue-stained femoral arteries at 4 days after injury in KLF5$^{Tgln-/-}$ mice or KLF5^{wt} mice. Blue staining area indicates endothelial denudation. *p < 0.05 versus KLF5^{wt} mice (uninjured). #p < 0.05 versus KLF5^{wt} mice (injured). (n = 6 for each group). (C) Representative photographs of immunofluorescence staining of CD31 (red) in carotid arteries of KLF5$^{Tgln-/-}$apoE$^{-/-}$mice or apoE$^{-/-}$mice fed with HFD for 12 weeks. Magnification, × 100. (D) HASMCs were transfected with pAd-GFP or pAd-GFP-KLF5 for 48 hr. miRNAs in HASMCs were extracted, and miRNA array was performed (n = 3). (E) HASMCs were transfected with pAd or pAd-KLF5 for 48 hr. miRNA expression was detected by real-time PCR (n = 6). *p < 0.05 versus pAd group. (F) HASMCs were treated with oxLDL for 24 hr. KLF5 expression was detected by western blotting (n = 3). **p < 0.01 versus 0 mg/L oxLDL group. (G) HASMCs were treated with oxLDL for 24 hr. miRNA expression was detected by real-time PCR (n = 6). *p < 0.05 versus control (Con) group.

We aimed to identify miRNAs that are regulated by KLF5 in human aortic SMCs (HASMCs) and might contribute to the endothelial dysfunction during atherogenesis.

RESULTS

VSMC-Specific Deficiency of KLF5 Ameliorates Wire-Induced Injury in Mouse Femoral Arteries

To test whether KLF5 expressed in VSMCs is responsible for endothelial injury, we performed a wire denudation injury in the femoral arteries of KLF5$^{Tgln-/-}$ (VSMC-specific knockout of KLF5) mice and littermate wild-type (WT) mice. First, VSMC-specific KLF5 knockout was confirmed in KLF5$^{Tgln-/-}$ mice, which showed that the expression of KLF5 was not affected in other tissues, such as endothelium, heart, and skeletal muscles (Figures S1A and S1B). We found that neointimal hyperplasia was significantly suppressed in KLF5$^{Tgln-/-}$ mice 14 days after injury (Figure 1A, left panel), indicating that KLF5 knockout decreased the proliferation of VSMCs, which is consistent with our previous findings.[8] In an experiment that followed, en face Evans blue staining of the denuded area of vessel wall showed that vascular endothelium of WT mice was severely damaged immediately after wire injury and recovered by ≈30% at day 4. In contrast, re-endothelialization in KLF5$^{Tgln-/-}$ mice was 65% at day 4 postinjury (Figure 1B). Moreover, KLF5$^{Tgln-/-}$apoE$^{-/-}$ mice exhibited apparently organized vascular endothelium compared with apoE$^{-/-}$ mice, further indicating an important physiological link between KLF5-regulated genes in VSMCs and the ECs in the vasculature (Figure 1C). These results prompted us to believe that KLF5 expressed in VSMCs could affect the function of ECs through some unknown mechanism(s).

KLF5 Regulates the Expression of Multiple miRNAs

Based on recent studies that found that vesicle-mediated transfer of miRNAs can mediate signals between cells, we hypothesized that KLF5 regulates miRNA expression and secretion in VSMCs, and in turn, miRNAs, as communication factors, mediate the link between VSMCs and ECs during atherosclerosis. To assess which miRNAs

are regulated by KLF5 in VSMCs, we transduced HASMCs with an adenoviral vector encoding KLF5, resulting in an increase in the KLF5 expression levels (Figure S1C). We first used miRNA microarray analysis to determine the profile of miRNAs expressed in both mock- and KLF5-transduced HASMCs. The results showed that a number of miRNAs were markedly affected by KLF5 overexpression in HASMCs (Figure 1D) (Table S1). Among them, 43 miRNAs were upregulated, and 36 miRNAs were downregulated. We next identified the expression of miRNAs with an established role in vascular biology using real-time PCR (Figure 1E). The expression of proinflammatory miRNAs, such as miR-155 and miR-146a, was significantly induced by KLF5 (Figure 1E). However, the differentiated smooth-muscle-enriched miR-143 and miR-145 were downregulated by KLF5 overexpression (Figure 1E). KLF5 also reduced the expression levels of miR-222 and miR-221, which are involved in EC dysfunction in the pathogenesis of atherosclerosis. Furthermore, miR-155 and miR-146a were upregulated by prolonged KLF5 overexpression (Figure S1E). To determine whether endogenous activation of KLF5 would result in a comparable miRNA signature, we exposed HASMCs to oxLDL, which resulted in a robust induction of KLF5 protein (Figure 1F) and mRNA expression (Figure S1E). oxLDL also significantly reduced miR-143/145 and miR-221/222 expression, whereas that of miR-155 and miR-146a was increased, which is consistent with the regulation of these miRNAs by KLF5 (Figure 1G). Time-dependent changes in the expression of miR-155, miR-146a, and miR-143/145 after the exposure of HASMCs to oxLDL yielded similar results to those induced by KLF5 overexpression (Figure S1F). These results prompted us to believe that the pro-atherogenic factor oxLDL induced the expression of many miRNAs by upregulating KLF5 expression.

KLF5 Induces the Enrichment of miR-155 in Extracellular Vesicles

Since it is known that miR-155 promotes a pro-atherosclerotic phenotype in macrophages,[9] we hypothesized that exosomes were involved in the transfer of miR-155. To test this hypothesis, we first isolated vesicles from the supernatants of pAd- and pAd-KLF5-transduced HASMCs. Quantitative analysis of electron micrographs showed that the diameter of the vesicles was heterogeneous, but most were between 60 and 130 nm, with a median size of 100 nm (Figure S2A), indicating that most of the isolated vesicles comprise exosomes but not larger apoptotic bodies. Western blotting also confirmed the presence of the known exosomal marker CD63 on the exosome surface (Figure S2B). Furthermore, we found that KLF5 was not detected in exosomes by western blot, further suggesting that KLF5 expressed in VSMCs regulates EC function in an indirect way (Figure S2C). We next used miRNA microarray analysis to compare the miRNAs in extracellular vesicles derived from pAd- and pAd-KLF5-transduced HASMCs. The results showed that the expression of 187 miRNAs was altered in exosomes derived from KLF5-overexpressing HASMCs by at least 1.5-fold (Table S2) compared with KLF5-normoexpressing cells. Among them, 36 miRNAs were upregulated (Figure 2A; Table S2). These results further demonstrated that KLF5 regulated miRNA secretion in HASMCs. To further study the influence of KLF5 on the regulation of miR-155 in extracellular exosomes, we isolated miRNA from the vesicles and the remaining concentrated supernatant and measured miRNA expression levels by real-time PCR (Figure 2B). KLF5 overexpression resulted in a 15.31-fold enrichment of miR-155 in extracellular vesicles (Figure 2B), whereas the remaining supernatant did not show an upregulation of miR-155 levels (Figure S2D). Furthermore, the induction of miR-155 in SMCs by oxLDL was indeed KLF5 dependent, as shown by KLF5 overexpression (Figure 2C) or knockdown using KLF5 small interfering RNA (siRNA) (Figure 2D). To further study the underlying mechanism, we analyzed the promoter of miR-155 and found one putative KLF-binding site in an evolutionarily conserved region 2.5 kb upstream of miR-155 (Figure S2E). Indeed, KLF5 bound to this part of the miR-155 promoter, as demonstrated using a chromatin immunoprecipitation (ChIP) assay (Figure 2E). Moreover, KLF5 and oxLDL activated a miR-155-promoter-driven luciferase reporter construct (Figure 2F). Mutation of the conserved KLF5-binding site blocked KLF5-dependent activation (Figure S2F) most. Combined, these results show that the overexpression or endogenous activation of KLF5 upregulates miR-155 expression and secretion in HASMCs.

SMC-Derived miR-155 Is Transferred to ECs via Exosomes

To determine whether miR-155 transfer was mediated by the release of exosomes and whether ECs could take up SMC-derived exosomes, we performed co-culture experiments with HASMCs and ECs in which the cells were separated by a membrane of 0.4-μm pore size to prevent direct cell contact or transfer of larger vesicles (Figure 3A, left panel). In this setup, fluorescein isothiocyanate (FITC)-labeled-miR-155-transfected HASMCs were placed in the upper chamber of a transwell co-culture system. ECs (Figure S3) were seeded in the lower chamber. As shown in Figure 3A, FITC-labeled-miR-155 in ECs was also significantly increased following KLF5 overexpression, especially with oxLDL treatment (Figure 3A, right panel; Figure S3). KLF5 silencing abrogated the inducing effect of oxLDL on miR-155 expression. Consistent with this finding, the pharmacological inhibition of sphingomyelinase, which is known to inhibit exosome generation, attenuated the transfer of FITC-miR-155 to ECs (Figure 3B), indicating that the miRNA transfer was mediated by actively formed exosomes and that KLF5 promoted the transfer of miR-155 from SMCs to ECs. To distinguish between membrane-enclosed miRNAs, miRNAs that might be attached to the outside of these vesicles from miRNAs in protein complexes, we investigated the mode of protection of miR-155 in HASMC supernatants. The results showed that the degradation of the proteins alone (with proteinase K) before RNase treatment did not affect miR-155 levels (Figure 3C). In contrast, treatment with the phospholipid membrane disruptor Triton X-100 before RNase treatment led to a near-complete degradation of miR-155, indicating that SMC-derived miR-155 was preferentially protected by extracellular vesicles (Figure 3C). To further study the mechanism whereby exosomes were taken up by ECs, we labeled SMC-derived exosomes with PKH67 (a green fluorescent cell linker dye with long aliphatic carbon tail) and incubated ECs with the labeled exosomes (Figure 3D). Confocal microscopy analysis showed that exosomes were taken up by the ECs at each time point observed,

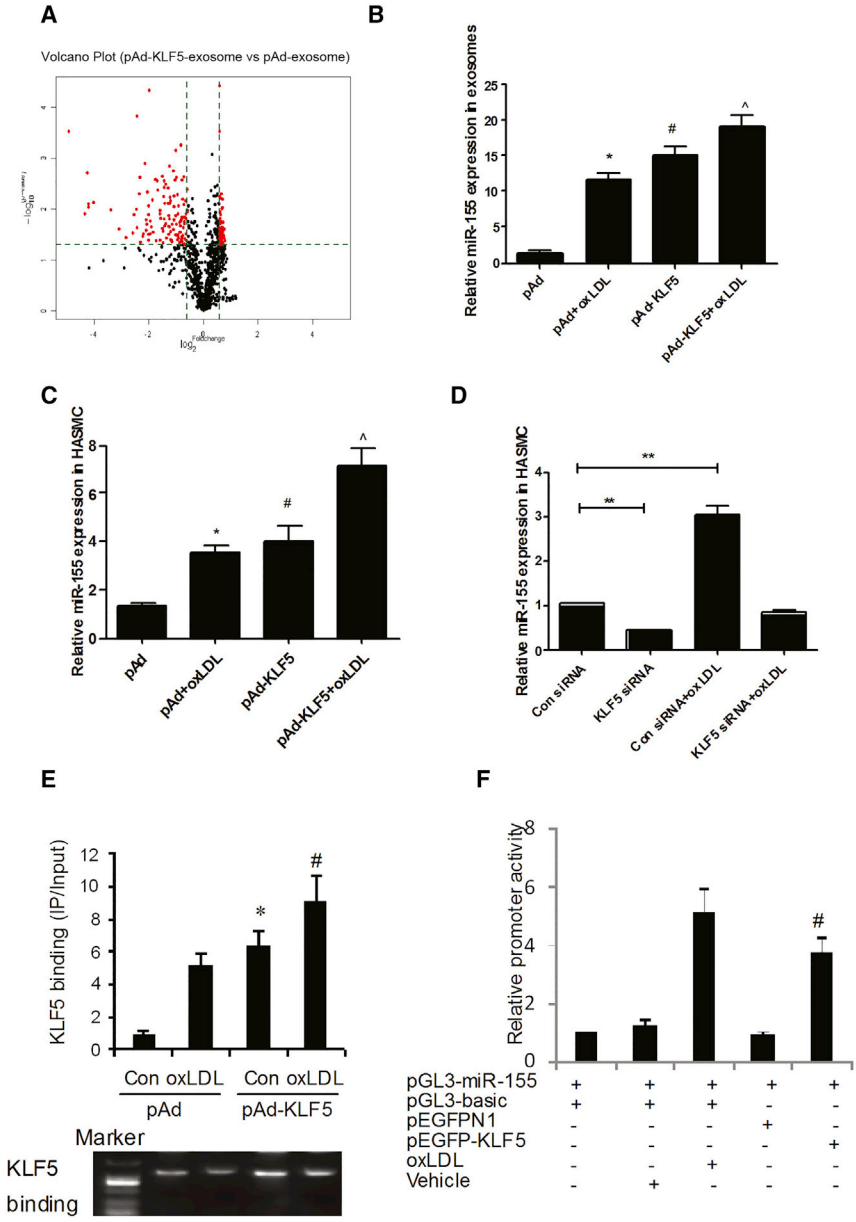

Figure 2. KLF5 Induces Enrichment of miR-155 in Extracellular Vesicles

(A) HASMCs were transfected with pAd or pAd-KLF5 for 48 hr. miRNAs from HASMC exosomes were extracted, and miRNA array was performed. (B) HASMCs were treated with oxLDL or transfected with pAd-KLF5 for 24 or 48 hr, respectively. Exosomes were extracted from the medium of VSMCs by ultracentrifuge. miR-155 expression in exosomes was detected by real-time PCR (n = 6). *p < 0.05 versus pAd group; #p < 0.05 versus pAd group; ^ p < 0.05 versus pAd-KLF5 group. (C) HASMCs were treated with oxLDL or transfected with pAd-KLF5 for 24 hr. miR-155 expression in HASMC was detected by real-time PCR (n = 6). *p < 0.05 versus pAd group; #p < 0.05 versus pAd group; ^p < 0.05 versus pAd-KLF5 group. (D) HASMCs were treated with oxLDL or transfected with KLF5 siRNA for 24 hr. miR-155 expression was detected by real-time PCR(n = 6). **p < 0.01 versus control (Con) siRNA. (E) ChIP assay for detecting the binding of KLF5 on miR-155 promoter. The result of real-time PCR is shown in the upper panel; the representative image of PCR products is shown in the lower panel. *p < 0.05 versus control; #p < 0.05 versus oxLDL. (F) Reporter gene assay using miR-155 promoter (n = 6). VSMCs were transfected with indicated vectors for 48 hr; luciferase activities were measured with the Dual-luciferase Reporter System (Promega). Results are means ± SEM for six separate transfection assays with duplicate plates. *p < 0.05 versus vehicle group; #p < 0.05 versus pEGFP N1 group (panel 5 versus panel 4).

especially with exosomes derived from KLF5-transduced HASMCs (Figure 3D). This finding was further supported by an increased level of miR-155 (Figure 3E) in ECs co-cultured with pAd-KLF5-transduced HASMCs, again suggesting that SMC-derived exosomes can be taken up by ECs and that KLF5 promotes exosome formation and transfer between SMCs and ECs.

SMC-Derived miR-155 Impairs Endothelial Integrity, Facilitating Atherosclerotic Plaque Formation

Based on our findings that KLF5 upregulated miR-155 expression and promoted the transfer of miR-155 from SMCs to ECs via exosomes, we sought to identify the role of miR-155 in ECs during atherogenesis. To this end, exosomes secreted by pAd-KLF5-transfected HASMCs (miR-155-rich exosome) or pAd-transfected HASMCs (con exosome) were injected into the tail veins of apoE$^{-/-}$ mice that were fed a high-fat diet (HFD) over a period of 12 weeks. We found that injection of miR-155-rich exosomes significantly increased the level of miR-155 in the aortas of apoE$^{-/-}$ mice (Figure 4A). The en face oil red O staining of the thoracoabdominal aorta showed that 18.2% ± 3.6% of the thoracoabdominal aortic area was covered with plaques in apoE$^{-/-}$ mice injected with miR-155-rich exosomes, relative to 11.3% ± 1.1% of the control exosomes (Figure 4B). To further detect the effect of miR-155-rich exosomes on early or advanced plaque, apoE$^{-/-}$ mice injection of exosomes was fed with HFD for 6 or 8 weeks. Oil red O staining of carotid artery sections (Figure 4C, left panel) showed that 36.4% ± 7.1% of the carotid artery area was covered with plaques in apoE$^{-/-}$ mice fed a HFD for 8 weeks injected with miR-155-rich exosomes, relative to 11.6% ± 0.9% of the control exosomes (Figure 4C, right panel). Accordingly, the miR-155 expression and distribution detected by fluorescence in situ hybridization (FISH) (Figure 4D, upper panel) were increased in the carotid artery plaque of apoE$^{-/-}$ mice injected with miR-155-rich exosomes. Meanwhile, the expression and distribution of CD31 (Figure 4D, upper

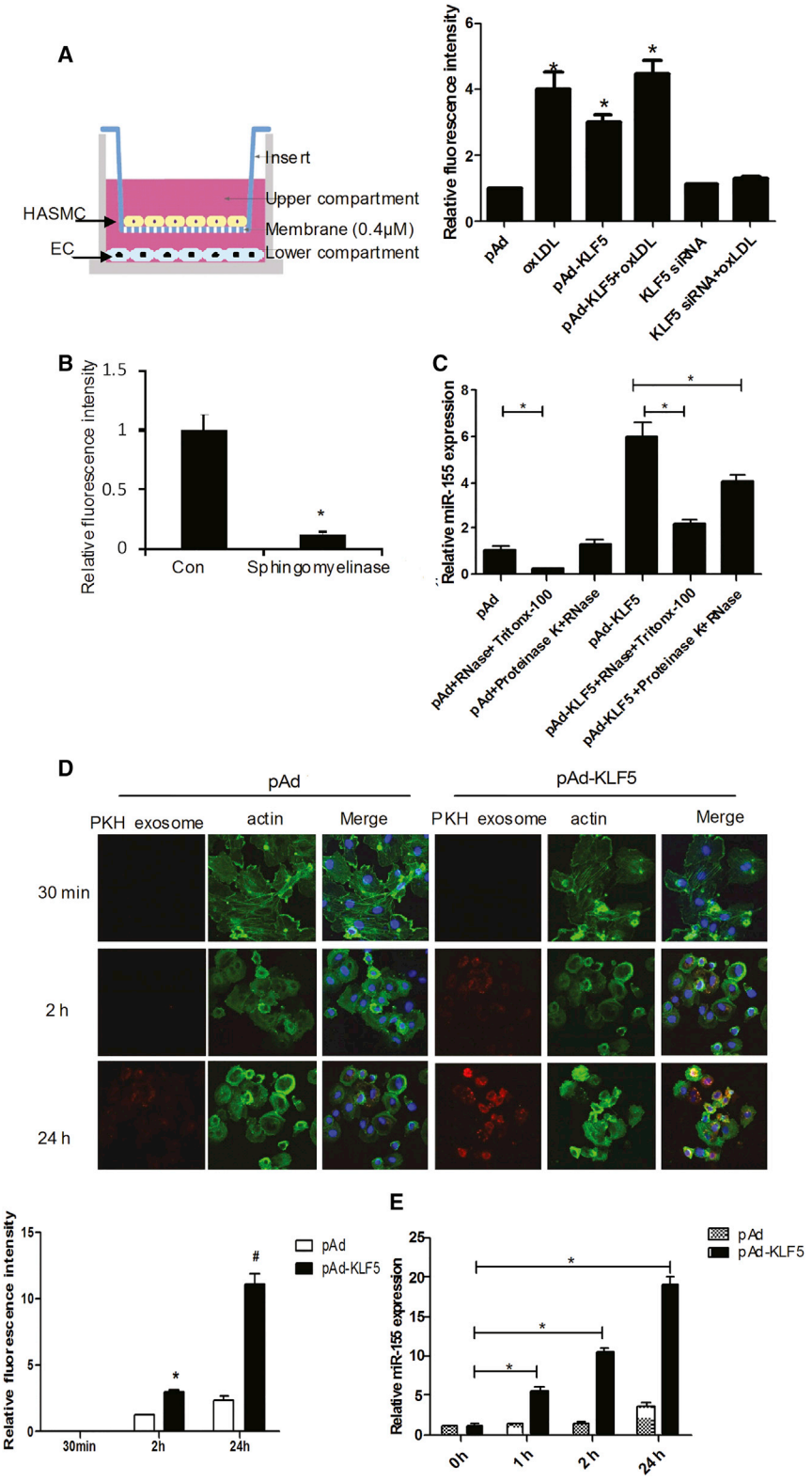

Figure 3. miR-155 in HASMCs Induced by KLF5 Can Be Transferred to ECS via Exosome Secretion

(A) An in vitro co-culture system was used where HASMCs are seeded in the top compartment, which is separated by a porous membrane from ECs that are cultured in the bottom compartment. HASMCs (top compartment) were transfected with FITC-miR-155 together with indicated virus or siRNA and treated with or without oxLDL and co-cultured with ECs (bottom compartment). FITC-miR-155 (green) and CD 31 expression (red) in ECs was analyzed by confocal microscopy. Statistical analysis of fluorescence intensity of FITC-miR-155 (right panel). *$p < 0.05$ versus pAd group. (B) HASMCs were seeded in the top compartment was treated with sphingomyelinase (10 μM) inhibitor, an inhibitor of exosome generation, then transfected with FITC-miR-155 together with indicated virus. Fluorescence intensity in ECs was detected using confocal microscopy. *$p < 0.05$ versus pAd group. (C) Extracellular vesicles of pAd or pAd-KLF5-transduced HASMCs were isolated and incubated with the indicated reagents for 45 min at 37°C before isolating RNA and measuring the levels of miR-155 of ECs by real-time PCR ($n = 6$). *$p < 0.05$. (D) ECs were incubated with the exosomes from PKH67-labeled (red) pAd- or pAd-KLF5 transduced HASMCs and fixed for confocal imaging. ECs were incubated with PKH67-labeled exosomes for 30 min, 2 hr, and 24 hr ($n = 4$) (upper panel). Exosome uptake was quantified as percentage of fluorescence intensity (lower panel). *$p < 0.05$ versus 2 hr of pAd transfection. #$p < 0.05$ versus 24 hr of pAd transfection. (E) ECs were incubated with the exosomes from PKH67-labeled (red) pAd- or pAd-KLF5 transduced HASMCs; real-time PCR detects the expression of miR-155 in ECs. *$p < 0.05$ versus 0 hr group.

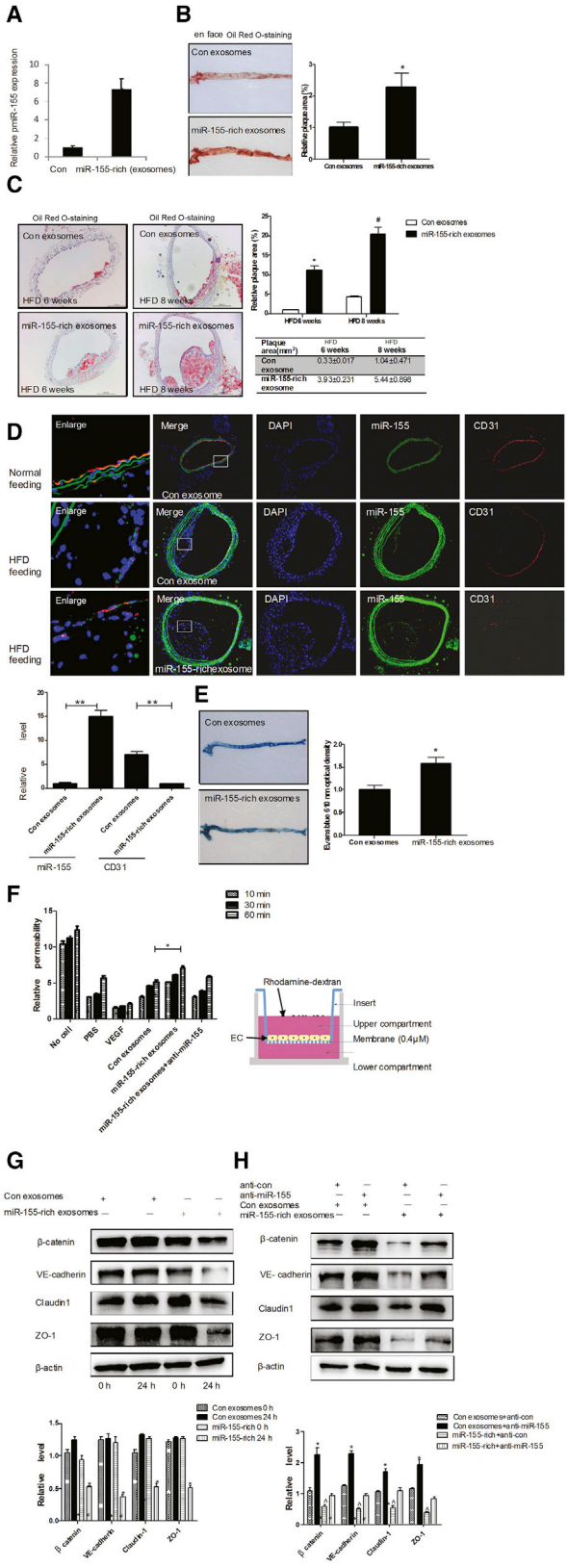

Figure 4. Vascular-Derived miR-155 Is Transported to ECs, Leading to Cellular Dysfunction

(A) Exosomes secreted by pAd or pAd-KLF5-transduced HASMCs were intravenously injected into the tail vein of apoE$^{-/-}$ mice fed with HFD (n = 6) once a week. After 12 weeks, total RNA from aortic arch vessels was isolated for real-time PCR of miR-155. **p < 0.01 versus control exosomes (con). (B) Exosomes prepared as above were intravenously injected into the tail vein of apoE$^{-/-}$ mice fed with HFD (n = 6) once a week. The atherosclerotic lesion areas in thoracoabdominal aorta of apoE$^{-/-}$ mice fed with HFD for 12 weeks were stained with en face oil red O (left panel). Quantitative analysis of the plaque areas (right panel). *p < 0.05 versus con exosomes. (C) Representative photographs of oil-red-O-stained carotid arteries of apoE$^{-/-}$ mice fed with a HFD for 6 or 8 weeks. The carotid sections were stained with oil red O (left panel). Quantitative analysis of the plaque areas (right panel). *p < 0.01 versus con exosomes. #p < 0.01 versus con exosomes (upper panel); plaque areas (lower panel). (D) Representative photographs of miR-155 in situ hybridization (green) or CD31 staining (red) (upper panel). Quantitative analysis of fluorescence intensity (lower panel). **p < 0.01 versus control exosomes. (E) Representative photographs of aorta of apoE$^{-/-}$ mice fed with a HFD for 12 weeks. The apoE$^{-/-}$ mice were anesthetized and 0.1 mL of 1% Evans blue (EB) dye was injected into the inferior vena cava. After 30 min, the blood vessels were perfused with PBS through the left ventriculum, and the aortas were isolated and photographed. After taking the pictures, the aortas were minced and incubated in formamide at 55°C for 24 hr, and the optical density was measured at 610 nm. The aortic endothelial permeability was expressed as nanograms of EB dye extravasated per milligram of tissue. *p < 0.01 versus con exosomes. (F) The permeability of EC monolayers grown on 0.4-μm filters was measured by the transmembrane transport of rhodamine-dextran, which was added to the top well at the beginning of the experiment, in the bottom well during a 1-hr time course. The absorbance at 590 nm was indicated. Treatment of the EC monolayer with VEGF (50 ng/mL) for 8 hr was included as a positive control to show cytokine-induced permeability. *p < 0.05 versus con exosomes. (G) Exosomes prepared as above were incubated with ECs for 24 hr. The expression of TJ proteins was detected using western blotting (upper panel), and band intensities were quantified by optical density scanning (lower panel). (H) Exosomes secreted by pAd-KLF5 and miR-155 inhibitor-transfected HASMCs were incubated with ECs for 24 hr. The expression of TJ proteins was detected using western blotting (upper panel), and band intensities were quantified by optical density scanning (lower panel).

panel) (Figure S4A) and mac-2 (Figure S4A) were detected. As shown in Figure 4D, CD31 expression was significantly decreased in apoE$^{-/-}$ mice injected with miR-155-rich exosomes compared with those injected with control exosomes (Figure 4D, lower panel). In contrast, mac-2 expression and SM α-actin expression were increased. Furthermore, en face Evans blue staining of plaque also showed that endothelial integrity was damaged severely in miR-155-rich exosome-injected mice (Figure 4E). These results suggest that one of the proatherogenic effects of miR-155 might be related to its impairment of endothelial function. Furthermore, we added miR-155-rich exosomes into cultured ECs and found that the proliferation (Figure S4B) and migration (Figure S4C) of miR-155-rich exosome-treated ECs were significantly decreased compared with the control. Accordingly, the inhibition of miR-155 using a miR-155 inhibitor counteracted the effect of miR-155-rich exosomes on endothelial proliferation and migration. Next, we used an in vitro angiogenesis assay to determine the effect of miR-155-rich exosomes on endothelial tube formation. The results showed that ECs coincubated with miR-155-rich exosomes lost their ability to form vessels, as evidenced by the fact that miR-155-rich exosome-treated ECs formed shorter and more

homogeneous tubules than those coincubated with control exosomes, suggesting that miR-155 exerts antiangiogenic effects on ECs (Figure S4D). These results in VSMCs identified that miR-155-rich exosomes could damage the endothelial function of KLF5.. The co-culture system further identified that overexpression of miR-155 in KLF5-induced SMCs decreased the proliferation and migration of ECs (Figures S4E and S4F). Accordingly, inhibition of miR-155 expression in SMCs using miR-155 inhibitor offset the effect of overexpression KLF5 on ECs (Figures S4E and S4F).

We next performed an in vitro permeability assay by measuring the migration of rhodamine-labeled dextran probes through EC monolayers growing on 0.4-μm filters. As shown in Figure 4F, treatment of the endothelial barrier with miR-155-rich exosomes induced the passage of the fluorescent probes from the top to the bottom wells in a time-dependent manner. Due to the fact that the permeability of the endothelial monolayer depends primarily on endothelial tight junctions (TJs), and that disruption of TJs facilitates lipid accumulation and plaque formation, we sought to examine whether miR-155-rich exosomes affected the expression of TJ proteins in ECs. Treatment of ECs with miR-155-rich exosomes but not control exosomes resulted in a significant decrease in the expression of TJ proteins, especially zonula occludens-1 (ZO-1) (Figure 4G). The inhibiting effect of miR-155-rich exosomes on TJ expression could be abolished by transfecting the recipient cells with a miR-155 inhibitor (Figure 4H). These results suggest that SMC-derived miR-155 impairs endothelial barrier function by suppressing the expression of TJ proteins.

miR-155 Disrupts the Endothelial Barrier by Decreasing TJ Protein Expression

Next, we further study the function of miR-155 on endothelial barrier and its mechanism. We found that, in response to HFD feeding, the aortas from miR-155$^{-/-}$apoE$^{-/-}$ mice showed decreased permeability, as determined by the extravasation of Evans blue dye when compared with the aortas from miR-155^{WT}apoE$^{-/-}$ mice (Figure 5A). miR-155 overexpression by pAd-miR-155 infection significantly decreased the expression of TJ proteins, such as ZO-1 and claudin 1, and adhesion molecules, including β-catenin and vascular endothelial (VE)-catenin, at both the protein (Figure 5B) and mRNA levels (Figure S5A). In contrast, the knockdown of miR-155 increased the expression of these proteins (Figure 5B, lane 4 versus lane 3).

An in vitro EC permeability assay further revealed that miR-155 overexpression using miR-155 mimics led to a loss of endothelial barrier function (Figure 5C). Using ECs, western blotting showed that the overexpression of miR-155 decreased the expression of TJ proteins. Accordingly, silencing of miR-155 by miR-155 inhibitor increased the expression of TJ proteins (Figure 5D). Immunofluorescence staining of β-catenin and VE-catenin revealed that these proteins were localized at the TJs between ECs after miR-155 blockade by its inhibitor, but they were dislocated from the TJs upon miR-155 overexpression (Figure 5E). We next examined the miR-155 regulation of the putative target ZO-1, a central molecular component of TJs, which compose a major group of cell-cell adhesion complexes in ECs. The predicted miR-155-binding site in the 3′ UTR of human ZO-1 was cloned into a reporter plasmid and assessed for their responsiveness to miR-155 in human microvascular endothelial cells (HMVECs). The level of reporter activity for ZO-1 was significantly lower in miR-155-expressing cells, whereas that of reporter activity for the mutated ZO-1 3′ UTR was unaffected (Figure 5F). However, different algorithms, such as miRecords, miRanda, and TargetScan 5.1, did not identify β-catenin, VE-catenin, or claudin 1 as miR-155 targets. We surmised that, although β-catenin, VE-catenin, and claudin 1 were not the direct targets of miR-155, the reduction of these proteins was affected by miR-155 indirectly. This question is the direction of our future research.

Deletion or Inhibition of miR-155 Suppresses Atherogenesis

We next determined whether the miR-155 level in SMCs was altered during atherogenesis. We found the expression of miR-155 in plaque was increased with the time of HFD feeding (Figure S6A). Meanwhile, as shown in Figures 6A and 6B, miR-155 expression (green) was significantly increased in the VSMCs (red) of atherosclerotic apoE$^{-/-}$ mouse tissue (Figure 6A) and in VSMCs of human atherosclerotic plaque tissue, as detected by a miRNA FISH assay (Figure 6B). Furthermore, we generated miR-155$^{-/-}$apoE$^{-/-}$ mice and detected whether the deletion of miR-155 affected atherosclerosis. The results showed that the plaque size and lipid deposition were significantly decreased in miR-155$^{-/-}$apoE$^{-/-}$ mice (0.16 ± 0.02) compared with miR-155^{wt}apoE$^{-/-}$ mice (1.32 ± 0.29) (Figures 6C and S6B). Additionally, the medial area was also different between the groups (miR-155^{wt}apoE$^{-/-}$ 5.12 ± 0.71 versus miR-155$^{-/-}$apoE$^{-/-}$ 0.51 ± 0.06) (Figures 6C and S6B). Moreover, the relative SMC content was decreased in miR-155$^{-/-}$apoE$^{-/-}$ mice (Figure 6D), but the relative EC content was increased by miR-155 deficiency (Figure 6D). These data suggest that the deletion of miR-155 suppresses atherosclerosis progression by facilitating EC proliferation. To further assess the effect of miR-155 on endothelial function in vitro, gain- and loss-of-function experiments were performed in ECs by transfecting the cells with either a miR-155 mimic or anti-miR-155. miR-155 mimic transfection markedly decreased EC proliferation (Figure S6C), angiogenesis (Figure S6D), and migration (Figure S6E), as assessed by an [3-(4,5-dimethylthiazol-2-yl)-5-(3-carboxymethoxyphenyl)-2-(4-sulfophenyl)-2H-tetrazolium (MTS) assay, a tube-formation assay, and a wound-healing assay. In contrast, anti-miR-155 (miR-155 inhibitor) transfection led to increased EC proliferation (Figure S6C), angiogenesis (Figure S6D), and migration (Figure S6E), suggesting that miR-155 impairs endothelial function by repressing EC proliferation and migration.

LNA-Anti-miR-155 Therapeutic Effect for Atherosclerosis

To determine whether the inhibition of miR-155 could prevent atherogenesis in a mouse model, apoE$^{-/-}$ mice were fed a HFD for 4 weeks to induce atherogenesis, followed by 4 weeks of treatment with LNA-anti-miR-155 (locked nucleic acid [LNA]-modified anti-miRNAs). The mice were then randomly assigned to receive LNA-anti-miR-155 or LNA control. LNA treatment (LNA control or LNA-anti-miR-155) had no impact on body weight during the

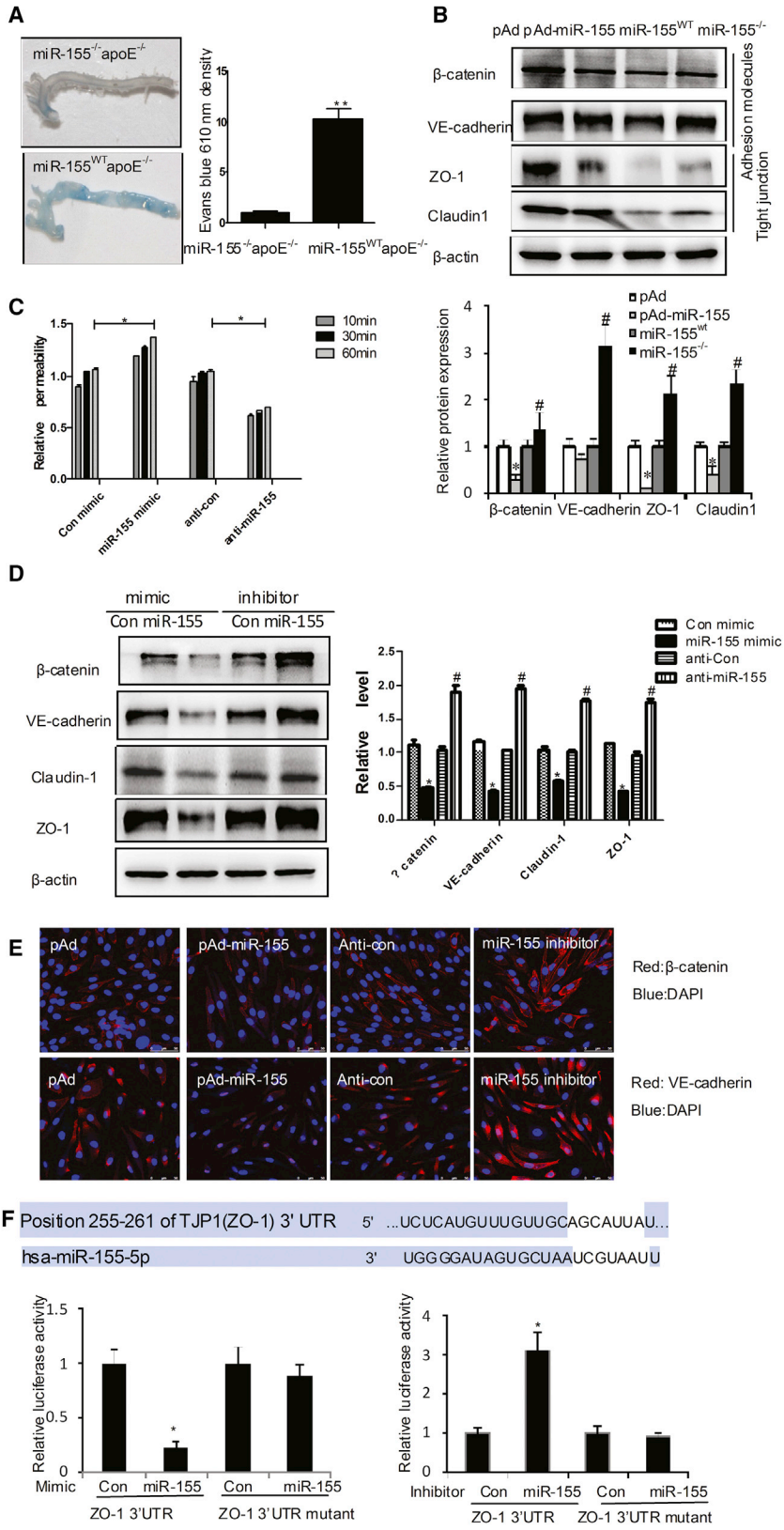

Figure 5. miR-155 Regulates Endothelial Barrier Function

(A) After feeding with HFD for 8 weeks, the apoE$^{-/-}$ or miR-155$^{-/-}$apoE$^{-/-}$ mice were treated, and the aortic endothelial permeability was determined as described in Figure 4E. (B) pAd or pAd-KLF5 was intravenously injected into the tail vein of C57BL/6 mice (n = 6) once a week. Protein extracts from aortic tissues of miR-155^{wt} or miR-155$^{-/-}$ mice (n = 6) were prepared, and indicated TJ proteins were detected by western blotting. Quantitative analysis of protein expression is shown in the lower panel. *p < 0.05 versus pAd group; $^{\#}$p < 0.05 versus miR-155^{wt} group. (C) The permeability of EC monolayers grown on 0.4-μm filters was measured as described above. (D) TJ protein expression was detected by western blotting in ECs transfected with miR-155 mimic or miR-155 inhibitor (anti-miR-155). Quantitative analysis of protein expression is shown in the right panel. *p < 0.05 versus control mimic; $^{\#}$p < 0.05 versus anti-control. (E) Representative photographs of immunofluorescence staining of TJ proteins in ECs transfected with pAd-miR-155 or miR-155 inhibitor. (F) 293A cells were co-transfected with miR-155 mimic or inhibitor together with pLuc-ZO-1-3′ UTR. Twenty-four hours later, cells were harvested for the determination of luciferase activities. Experiments were performed in triplicate and each value is the mean ± SEM of three independent experiments. *p < 0.05 versus control.

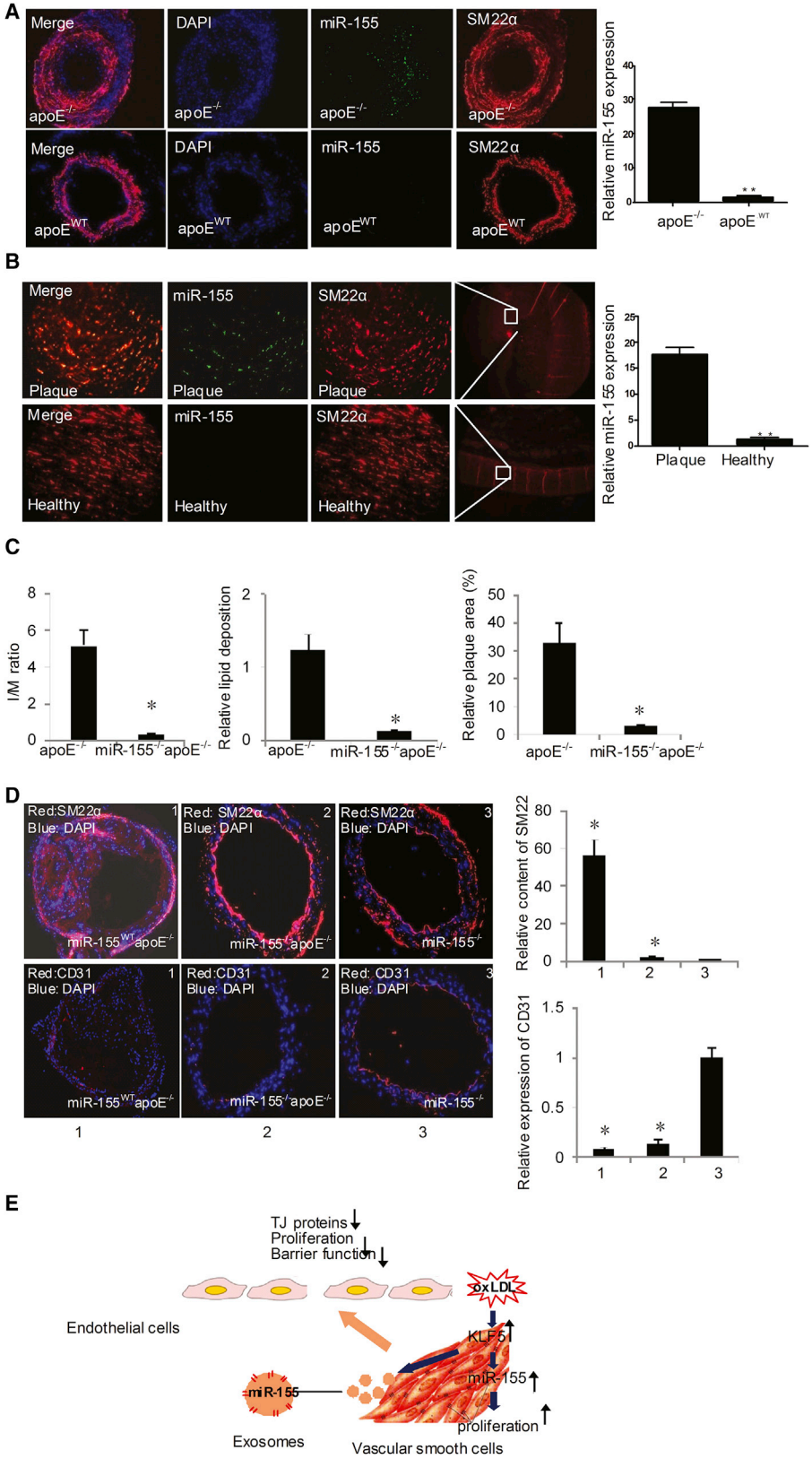

(legend on next page)

study period. We also assessed the inhibition of miR-155 by FISH (Figure S7). Notably, treatment with LNA-anti-miR-155 efficiently blocked atherogenesis (Figure 7A) and restored the vascular integrity (Figure 7B) and CD31expression in vascular ECs (Figure 7C), as detected by oil red O staining, Evans staining, and immunofluorescence staining, respectively. These results imply that anti-miR-155 treatment suppresses atherogenesis by restoring the barrier function of vascular endothelium. To further examine whether targeting miR-155 might reverse established disease, apoE$^{-/-}$ mice were fed a HFD for 8 weeks to induce atherosclerosis followed by treatment with LNA-anti-miR-155 for another 4 weeks. The results showed that targeting miR-155 could not completely reverse established atherosclerosis (Figure 7D) by oil red O staining. However, LNA-anti-miR-155 could improve the endothelium function (Figure 7E).

DISCUSSION

Exosomes have recently emerged as important players in intercellular communication.[10] Recent findings have suggested that different cell types can secrete or receive miRNAs as a form of communication and have set the stage for investigating the functional roles of transferred miRNAs in the context of immune responses.[11] In this study, our data demonstrate that KLF5 exerted its pro-atherosclerotic effect by regulating the expression of multiple miRNAs, most prominently miR-155. We found that miR-155-rich exosomes were secreted from KLF5-overexpressing VSMCs and were taken up by recipient ECs. Upon uptake by ECs, miR-155 inhibited the proliferation and migration of ECs and impaired endothelial barrier function by suppressing the expression of TJ proteins. Our results indicate that miR-155 acts as a communication molecule between SMCs and ECs to coordinate the responses of these two cells to pro-atherosclerotic factors. Thus, targeting KLF5 or miR-155 in combination with existing conventional therapies might be a novel therapeutic strategy in atherosclerosis.

KLF5 is an important transcription factor that regulates a number of cellular processes, including development, differentiation, proliferation, and apoptosis.[12] In the cardiovascular system, KLF5 is a target for AngII signaling and is an essential regulator of cardiovascular remodeling.[3] Some previous studies demonstrated that expression of KLF5 in mature VSMCs is upregulated by various pathological stimuli, including coronary atherosclerosis, vein graft, and vascular injury.[13–15] In this study, our results show that oxLDL, which is a potent pro-atherosclerotic factor, stimulates the expression of KLF5 in VSMCs and impairs the function of ECs. VSMC-specific knockdown of KLF5 can decrease neointimal hyperplasia and endothelial injury in the wire-injured femoral arteries of apoE$^{-/-}$ mice. These results showing that KLF5 expressed in VSMCs can lead to endothelial injury prompted us to investigate how KLF5 expressed in VSMCs exerts its regulatory effects on endothelial function. In this regard, it is noteworthy that the shear-responsive transcription factor Krüppel-like factor 2 (KLF2) is a critical regulator of endothelial gene expression induced by fluid shear stress.[16] Hergenreider et al. found that endothelial overexpression of KLF2 induces the expression and secretion of miRNAs that regulate SMC phenotypes in co-culture systems.[17] They further confirmed that miR-143/145 secreted by KLF2-transduced or shear-stress-induced HUVECs enriched in exosomes and regulated target gene expression in co-cultured SMCs.[17] The exosomes derived from KLF2-expressing ECs also induced atherosclerotic lesion formation. These results suggest that miRNA-rich exosomes can mediate communication between ECs and SMCs. Two closely related both KLF5 and KLF2 are members of Krüppel-like factor family. They have a similar structure but different functions. The results that KLF2-induced miR-143/145 mediate communication between ECs and SMCs prompted us to believe that KLF5-induced miRNAs in SMCs could also regulate endothelial function by an exosome-mediated mechanism.

In the process of atherosclerosis, oxLDL stimulate phagocytosis, which reduces intercellular direct communication. Accumulation of lipids internalized by phagocytosis leads to isolation of cell disruption of cell-to-cell gap junction and contacts and to the disintegration of the cellular network.[18] The destruction of cell-to-cell contact stimulates VSMC and macrophage proliferation and extracellular matrix production; the latter isolates a cell from the neighboring cells. Therefore, exosomes have one of the pivotal roles in cellular communication.

miRNA array results showed that miR-155 was enriched in exosomes deprived from KLF5-overexpressing VSMCs. Further observation found that miR-155 expressed in VSMCs was secreted to surrounding ECs or macrophages by exosomes, which promoted atherosclerosis. Indeed, our previous study has demonstrated that miR-155, which is an inflammation-related miRNA, is unregulated in macrophages,[19] meaning that KLF5 and miR-155 could co-operatively promote atherosclerotic development.

The endothelium forms a selective permeability barrier between the vascular wall and blood.[20] Cell-to-cell connections, such as adherents junctions (AJs), TJs, and gap junctions, play important roles in the regulation of endothelial barrier function, and their disruption perturbs endothelial barrier function and promotes inflammation.[21] Endothelial dysfunction is generally regarded as the initial step in

Figure 6. miR-155 Inhibition Suppresses Atherogenesis

(A) Immunofluorescence staining of miR-155 (green) and SM22α (red) in apoE$^{-/-}$ mouse atherosclerotic or normal carotid artery tissues after being fed with HFD for 12 weeks. Magnification, × 100. (B) Immunofluorescence staining of miR-155 (green) and SM22α (red) in the human atherosclerotic or normal carotid artery tissues. Magnification, ×100. (C) Quantitative analysis of I/M ratio, lipid deposition, and relative plaque area of apoE$^{-/-}$ or miR-155$^{-/-}$apoE$^{-/-}$ mice. (D) Representative photographs of immunofluorescence staining of the SMC-specific marker SM22α and endothelial-specific marker CD31 in the carotid artery tissues of apoE$^{-/-}$ or miR-155$^{-/-}$apoE$^{-/-}$ mice. Magnification, ×100. The number of SMCs and ECs in the plaques was quantified. Means of all of the mice of one group (n = 6) are shown with SEM. *$p < 0.05$ versus miR-155$^{-/-}$ group. (E) Model of the function of miR-155-rich exosomes.

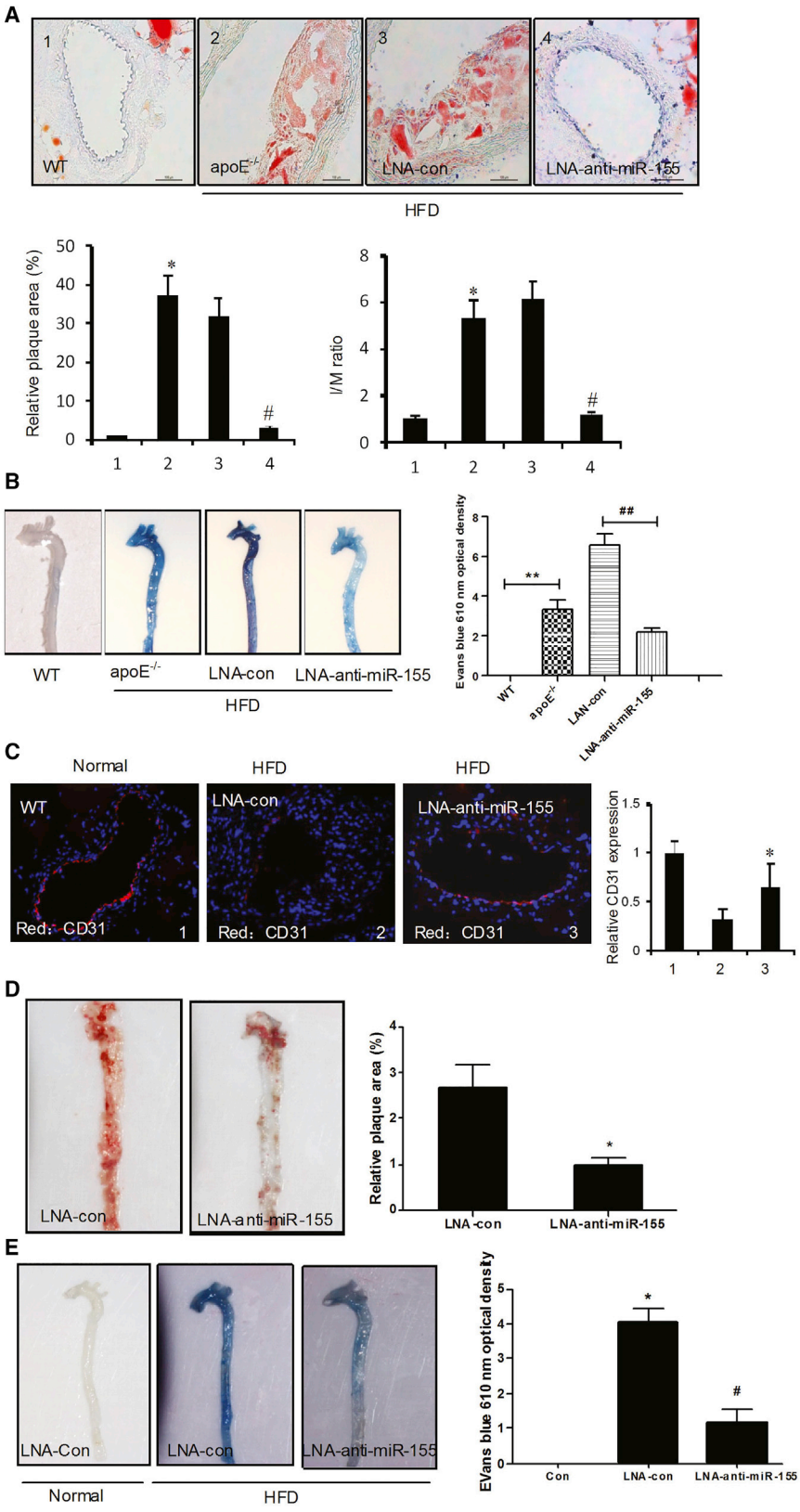

Figure 7. Inhibition of miR-155 Prevents Atherogenesis

After feeding with HFD for 4 weeks, the WT and apoE$^{-/-}$ mice were treated with LNA-con or LNA-anti-miR-155 for another 4 weeks. (A) Representative photographs of oil-red-O-stained carotid artery tissues (upper panel). Quantitative analysis of plaque areas and ratio of I/M in all mice of one group are shown with the SEM (n = 6) (lower panel). *p < 0.05 versus WT group; #p < 0.05 versus LNA-anti-con group. (B) The aortic endothelial permeability was determined as described in Figure 4E and expressed as nanograms of EB dye extravagated per milligram of tissue (right panel). (C) Immunofluorescence staining of CD31(red) in atherosclerotic or normal carotid artery tissues (left panel). Quantitative analysis of CD31 expression (left panel). *p < 0.05 versus LNA-con group (right panel). ApoE$^{-/-}$ mice were fed for 8 weeks to induce atherosclerosis and were then treated with LNA-anti-miR-155 for another 4 weeks. (D) The atherosclerotic lesion areas in thoracoabdominal of apoE$^{-/-}$ mice were stained with en face oil red O (left panel). Quantitative analysis of the plaque areas. *p < 0.05 versus LNA-con group (right panel). (E) The aortic endothelial permeability was determined as described in Figure 4E (left panel) and expressed as nanograms of EB dye extravagated per milligram of tissue (right panel). #p < 0.05 versus LNA-con group (right panel).

atherosclerotic plaque formation. oxLDL is a key element in the development of atherosclerosis. It can result in endothelial dysfunction via multiple mechanisms, including EC apoptosis, disrupting cell-to-cell junction and increasing endothelial permeability,[22] etc. In the present study, we have added a novel mechanism whereby oxLDL-induced KLF5 upregulates miR-155 expression in VSMCs, and then VSMC-derived miR-155 is transferred to ECs via exosomes and exerts its damaging effect on ECs. Our study identified that miR-155 could inhibit the expression of TJ proteins, especially ZO-1. In ECs that normally express low miR-155 levels, ectopic, SMC-derived miR-155 transferred via exosomes can effectively reduce ZO-1 expression, disrupt the barrier function of vascular endothelium both in vitro and in vivo, and open "gates" in these natural monolayer barriers for the traversal of macrophages, thereby facilitating atherosclerosis. Notably, abnormal miR-155 expression is involved in the occurrence of diseases such as cancer, cardiovascular disease, and inflammation.[9,23]

Downregulation or loss of TJs, frequently as a result of the reduced expression of TJ-associated proteins, contributes to atherosclerosis progression by altering cell migration and proliferation.[24] In ECs, Zhu et al. found that miR-155 is upregulated by high shear stress and targets the angiotensin II type 1 receptor and Ets-1, thus reducing the proinflammatory activity of angiotensin II.[25] In addition, miR-155 can also contribute to the formation of foam cells and enhance atherosclerosis progression.[9] Nazari-Jahantigh et al. demonstrated that miR-155 promotes flow-induced atherosclerosis by enhancing the inflammatory macrophage response, exemplified by CCL2 expression.[9] miR-155 also plays a proatherogenic role in proinflammatory M1-type macrophages in advanced atherosclerosis. In our previous study, we found that, in marrow-derived macrophages, miR-155 and tumor necrosis factor-α (TNF-α) formed a positive feedback loop to promote the inflammatory response.[19] In VSMCs, mammalian sterile 20-like kinase 2 (MST2) mediates miR-155-promoted inflammatory and oxidative stress responses by altering the interaction of MEK with Raf-1 and MST2 in response to vascular injury.[26] Our study found that macrophages also could uptake the miR-155-rich exosomes secreted by KLF5-overexpressed VSMCs (data not shown), indicating that the communication between macrophages and VSMCs by miR-155-rich exosomes is also related to atherogenesis induced by KLF5 overexpression in VSMCs. Interestingly, Wang et al. identified that activated macrophages secrete miR-155-enriched exosomes as a paracrine regulator for fibroblast proliferation and inflammation.[27] In this study, we identified miR-155 as a key regulator of claudin 1, beta-catenin, and VE-cadherin, and especially ZO-1, suggesting a mechanism of TJ disruption associated with atherosclerosis progression. Thus, we propose a model for the role of miR-155 in endothelial dysfunction and atherogenesis in which VSMCs, in response to unfavorable conditions such as oxLDL exposure, release miR-155 via exosomes into the surrounding environment, which, in turn, suppresses TJ protein expression and thus disrupts the endothelial barrier, subsequently contributing to atherosclerosis. Altogether, these findings further illustrated that ECs, macrophages, and SMCs communicate with each other through exosomes in response to environmental cues.

Many findings emerged from this study. First, exosomes derived from KLF5-transduced cells are enriched in miR-155. KLF5 regulated miR-155 expression and secretion in HASMCs. The transfer of miRNAs is an important mechanism forming a synergic relationship between VSMCs and ECs during atherosclerosis. These data help elucidate a novel mechanism of KLF5-regulating cell communication in a miR-155-dependent manner. Second, transferred miR-155 influenced the responses of ECs to a lipid stimulus, impaired EC proliferation, decreased the expression of TJ proteins on the cell membrane, and regulated microvascular permeability. Third, therapies targeting miR-155 in combination with existing conventional therapies may serve as an effective treatment for atherosclerosis patients. This study elucidates a novel cellular and molecular pathway that influences miR-155 expression, and transfer between different cell types could lead to the development of new therapeutic approaches and new insights into atherosclerotic pathophysiology.

Conclusions

Problem

SMCs and ECs in the vasculature are involved in dysfunction of vascular cells during atherogenesis, although the mechanism by which these cell types communicate with each other in response to environmental cues remains incompletely understood.

Results

Exosomes derived from KLF5-transduced cells are enriched in miR-155. KLF5 regulated miR-155 expression and secretion in HASMCs.

Transferred miR-155 influenced the responses of ECs to a lipid stimulus, impaired EC proliferation, decreased the expression of TJ proteins on the cell membrane, and regulated microvascular permeability.

Therapies targeting miR-155 in combination with existing conventional therapies may serve as an effective treatment for atherosclerosis patients.

Impact

Blockade of the exosome-mediated transfer of miR-155 between different cell types may serve as a therapeutic target for atherosclerosis.

MATERIALS AND METHODS

Animals

ApoE$^{-/-}$ mice, miR-155 mutant mice, and Tgln-cre mice were purchased from Jackson Laboratory, and KLF5-flox mice were a gift from Huajing Wan (Wuhan University, China).[28] KLF5$^{-/-}$ mice were generated by crossing KLF5-flox mice and *Tgln-cre mice (SM-specific cre)*. *apoE*$^{-/-}$KLF5$^{\mathrm{Tgln}-/-}$ double-knockout mice were generated by crossing *apoE*$^{-/-}$ and KLF5$^{-/-}$ mice. The mice were housed in the Hebei Medical University animal facilities on a 12-hr light-dark cycle (7 a.m. to 7 p.m., light) in specific pathogen-free caging. The mice were weaned at 3–4 weeks of age, and all experiments

were performed on animals older than 8 weeks of age. The mice had ad libitum access to food and water except under fasting conditions. The model mice were fed a HFD (21% crude fat, 0.15% cholesterol, 19.5% casein) throughout the experiment for 3 months. Adenoviral constructs (1×10^9 plaque-forming units [PFUs]; empty, KLF5) were injected via the tail vein every 14 days. An intraperitoneal injection of pentobarbital (5%) or the aerosol delivery of methoxyflurane was used for anesthesia. Blood samples were drawn from the retroorbital venous plexus or by direct transventricular catheterization into EDTA tubes, and the plasma was separated by centrifugation. The aortic tissue was immediately snap-frozen in liquid nitrogen for RNA extraction or cryopreserved in optimal cutting temperature compound (OCT) for further analysis. The excised aortic roots, abdominal aortas, and thoracic aortas (comprising the aortic arch and the proximal portion of the descending aorta) were washed in PBS, post-fixed in buffered formalin (4% formalin in PBS), and then embedded in paraffin.

Adenoviral Vectors

The construction of Ad-GFP and Ad-miR-155 was described previously.[26] Wherever adenoviral vectors were used, the cells were transduced with the indicated adenovirus at a multiplicity of infection (MOI) of 40 overnight in complete medium. After transduction, the cells were allowed to reach to 70% confluence in complete medium and growth-arrested for 24 hr before use.

Analysis of Stained Sections

Plaque extensions on tissue sections of the carotid artery were evaluated on pentachrome-stained sections, and lipid core sizes were determined by measuring the area of oil red O staining. The carotid artery was embedded with OCT and then made into 5-μm frozen sections. Formalin-fixed, paraffin-embedded tissues sectioned at 4-μm were analyzed by H&E staining for morphology. Arterial specimens were sectioned to identify the region with maximal luminal narrowing. These sections were selected for morphometric measurement of the medial area, the intimal area, and the intima/media (I/M) ratio. The sections were visualized using a Leica light microscope (Leica Microsystems). A minimum of eight mice per genotype were analyzed for the morphometric measurements. Protein expression and distribution were detected by immunohistochemistry. The antibodies used included monoclonal anti-KLF5 (1:100; Abcam), monoclonal anti-SM-actin (1:500; Sigma), polyclonal anti-SM-actin (1:100; Abcam), polyclonal anti-CD31 (1:100; Abcam), and polyclonal anti-mac-2 (1:200; Abcam).

Cell Culture and Transfection

HASMCs (5×10^5 cells in 6-well plates), cultured in DMEM supplemented with 10% fetal bovine serum, were transfected with 10 nmol/L of the miRIDIAN mimic miR-155 (Thermo Fisher Scientific) or the inhibitor miR-155 using the Lipofectamine 2000 reagent (Invitrogen) according to the manufacturer's instructions. The human cardiac microvascular endothelial cell (HCMECs) line (catalog no. 6110) was from ScienCell and was cultured in EC medium with 10% fetal bovine serum and maintained in 5% CO_2 at 37°C in a humidified atmosphere.

RNA Isolation, Reverse Transcription, and Real-Time PCR

The total RNA from the aortas of the ApoE$^{-/-}$ mice or HASMCs was isolated using the RNAqueous kit (Ambion). The RNA purity and concentration were assessed in an UV spectrophotometer (Thermo Scientific). RT was performed with the High-Capacity cDNA Archive Kit (Applied Biosystems) according to the manufacturer's procedure. For mouse KLF5, the forward primer is 5′-ACCATTTTCAGCCA CCAGAG-3′, and the reverse primer is 5′-GTCTGGTGGGAGC TGAAGA-3′. For β-actin, the forward primer is 5′-GTGGGCCG CTCTAGGCACCAA-3′, and the reverse primer is 5′-CTCTTTGA TGTCACGCACGATTTC-3′. All miRNAs were extracted from the aortas of the ApoE$^{-/-}$ mice, from the serum of human CAD patients, and from control individuals using the miRNeasy Mini Kit (QIAGEN) and reverse-transcribed with the RT2 miRNA First Strand Kit (QIAGEN) according to the manufacturer's instructions. Real-time PCR was performed on a StepOnePlus Real-Time PCR System (Applied Biosystems) using the RT2 SybrGreen quantitative PCR Mastermix (QIAGEN). To amplify mature miRNA sequences, TaqMan MicroRNA Assays hsa-miR-155 (Assay ID 12601), U6 snRNA (Assay ID 001973), the TaqMan MicroRNA Reverse Transcription Kit (PN4366596), and TaqMan Universal PCR Master Mix No AmpErase UNG (PN4324018) were used. The real-time PCR amplifications were carried out in an ABI 5700 fast system and analyzed with the Sequence Detector Software version 2.1 (Applied Biosystems). The relative quantification of gene expression was performed using the comparative Ct method.[12]

MTS Assay

The cell growth rates were evaluated by the tetrazolium-dye-based MTS assay, as described previously.[12] In brief, 1×10^4 cells/well were seeded in triplicate into 96-well plates in DMEM. After 24 hr, the cells were treated according to the experimental design. After each treatment, the medium was removed, and the cells were washed in PBS. The MTS reagent was added at 2 mg/mL in Hank's buffer and incubated for 1 hr until dark-blue crystals could be seen in the cytoplasm under light microscopy. The crystals were dissolved in DMSO, and the absorbance was measured in a Thermo Fluoroscan Ascent spectrometer at 570 nm with background subtraction at 650 nm. The results were expressed as the means ± SEM of the absorbance relative to time 0 or the control.

Exosome Purification and Electron Microscopy

Exosomes were isolated and purified from the supernatants of HASMC cultures using differential centrifugation. The HASMCs were cultured in DMEM-containing exosome-depleted serum. After 72 hr, the medium was collected and centrifuged at $2,000 \times g$ for 15 min at 4°C and then again at $12,000 \times g$ for 45 min at 4°C. The supernatants were then passed through a 0.22-μm filter (Millipore) and ultracentrifuged at $110,000 \times g$ for 90 min at 4°C. The pellets were then washed with phosphate-buffered saline (PBS) followed by a second ultracentrifugation at $110,000 \times g$ for 90 min at 4°C and then resuspended in PBS. The protein levels of the exosome preparations were measured using the BCA Protein Assay kit (Pierce) following the manufacturer's instructions. Exosome labeling with

PKH67 (Sigma) was performed following the manufacturer's procedures. The pelleted exosomes were resuspended in approximately 100 μL of PBS and subjected to electron microscopy (EM), cell treatment, or RNA extraction by mirVana miRNA isolation kit (Life Technologies). For EM, the exosomes were fixed with 2% paraformaldehyde, loaded on 200-mesh Formvar-coated grids, and then contrasted and embedded. The grids were observed under an transmission electron microscope equipped with a charge-coupled device (CCD) camera.[29]

Femoral Artery Wire Injury

Twelve-week-old male mice were used for all of the vascular injury experiments.[5] To induce neointima formation, the right femoral arteries underwent wire-induced injury using a 0.015-inch-diameter fixed-core wire guide (Cook) as previously described.[5] Immediately following injury, an adenoviral construct (MOI, 100; empty, KLF5) was infused and incubated for 15 min. Ten days following injury, the right injured and left uninjured femoral arteries were harvested, perfusion-fixed in 4% paraformaldehyde, and embedded in paraffin (ten sections, at 4 μm apart). Re-endothelialization of the femoral artery was determined by Evans blue staining 5 or 7 days after wire injury in mice.[30]

Animal Experimentation

All procedures involving animals were conducted according to the European Community guidelines (Directive 2010/63/EU). These animals were bred and maintained, and all procedures were performed under a protocol approved by the Institutional Animal Care and Use Committee at Hebei Medical University.

Western Blotting

Proteins were isolated from VSMCs as previously described and then separated by SDS-PAGE and transferred onto polyvinylidene difluoride membranes (Millipore).[31] The membranes were blocked with 5% milk in Tris-HCl Tween buffer solution for 2 hr at 37°C and incubated overnight at 4°C with a specific rabbit anti-Klf5 antibody (1:500, Abcam). The membranes were then incubated for 1 hr at room temperature with a 1:5,000 dilution of anti-rabbit/horseradish peroxidase or anti-mouse/horseradish peroxidase (Santa Cruz Biotechnology) and developed with the Chemiluminescence Plus Western Blot Analysis kit (Santa Cruz Biotechnology).

Immunofluorescence

Human cardiac microvascular endothelial cells (HAVECs) were grown to confluent monolayers on cell-culture-grade glass coverslips and treated with or without miR-155 inhibitors or pre-miR-155 mimics. After treatment, the cells were washed with cold PBS, fixed with 4% paraformaldehyde for 10 min at 4°C, permeabilized in Tris-buffered saline (TBS; 10 mM Tris-HCl [pH 8.0], 150 mM NaCl) containing 0.1% Triton X-100 for 10 min at room temperature and blocked in 2% BSA in TBS with 1.33 g/L $CaCl_2$, 1 g/L $MgCl_2$, and 0.1% saponin overnight at 4°C. Then, the cells were incubated with the desired primary antibodies followed by Alexa-Fluor-conjugated secondary antibodies. Fluorescence images of the cells were captured using an inverted Leica fluorescence microscope (IX71) or a Leica SP-8 confocal microscopic system.

ISH was performed in formaldehyde-fixed, paraffin-embedded tissue sections using a miRCURY LNA microRNA ISH optimization kit and the miR-155 detection probe (Exiqon) following the manufacturer's protocol. Probes for U6 and a scrambled sequence were used as positive and negative controls, respectively.

Luciferase Assay: 3′ UTR Reporter Assays

HASMCs were transfected with 30 pmol of pre-miR-Ctrl or pre-miR-155. The next day, the cells were transfected with 0.1 μg of the psiCHECK2 vector (Promega) expressing the 3′ UTR of the human ZO-1 mRNA or the mutated 3′ UTR of the human ZO-1 mRNA (QuikChange II Site-Directed Mutagenesis Kit, Agilent) with JET-PEI (Polyplus transfection) according to the manufacturer's instructions. After 24 hr, the luciferase assay was performed using the Dual-Luciferase Reporter Assay System (Promega). *Renilla* luciferase activity was normalized to firefly luciferase activity.[21]

Bioinformatic Analysis of the pri-miR-155 Promoter

Nucleotide sequences for *Homo sapiens* and eight orthologous sequences were obtained for the upstream region of the pri-155 promoter from the Ensembl database (assembly GRCH37.p8). Upstream regions were taken as 2,500 bases upstream and 500 bases downstream of the transcription start site. The identification of evolutionarily conserved transcription factor binding sites was performed using PhyloGibbs, a Gibbs sampling technique that utilizes phylogenetic footprinting. Secondary identification of transcription factor binding sites was performed using JASPAR and ConSite. J.

ChIP Assay

VSMCs were cross-linked with 1% formaldehyde for 15 min, lysed as previously described, and then sonicated to an average size of 400–600 bp.[32] The DNA fragments were immunoprecipitated overnight with anti-KLF5 or anti-mouse immunoglobulin G (IgG) (as a negative control). After the reversal of cross-linking, the pri-miR-155-flanking genomic region containing KLF5-binding sites was amplified by PCR; the forward and reverse primers used are shown in the Supplemental Information.

Boyden Chamber Assay

HAVECs transfected with and without miR-155 inhibitors or pre-miR-155 mimics were seeded in 8-μm 24-well Boyden chambers (Transwell; Costar Corp) and subjected to cell invasion assays. The lower chamber was filled with 600 μL of complete DMEM, and transfected HAVECs cells were placed in 300 μL of serum-free DMEM in the upper chamber and allowed to migrate for 4 hr at 37°C. After fixation, the cells were stained with 4% Giemsa and counted on the lower side of the membrane using ImageJ software.

Miles Assay

The level of vascular permeability was determined by quantitative measurement of the Evans blue dye diffusion into the aorta according

to the Miles test. miR-155$^{-/-}$, apoE$^{-/-}$, and miR-155$^{-/-}$apoE$^{-/-}$ mice fed a HFD for 8 weeks were anesthetized, and 0.1 mL of 1% Evans blue dye was injected into the inferior vena cava. After 30 min, the blood vessels were perfused with PBS through the left ventriculum, and the aortas were isolated. Evans blue dye was extracted from the arteries by incubating in formaldehyde at 55°C for 24 hr and then cleared by centrifugation, and the optical density was measured at 610 nm. Vascular permeability was expressed as the amount of Evans blue extravasated per milligram of artery.

Endothelial Permeability Assay

The permeability of treated HAVEC monolayers grown on transwell filters (0.4-μm pore size; BD Biosciences) was assessed by the passage of rhodamine B isothiocyanate-dextran (average molecular weight [MW] approximately 70,000; Sigma). Briefly, rhodamine-dextran was added to the top well at 20 mg/mL, and the appearance of fluorescence in the bottom well was monitored by measuring 40-μL aliquots in a time course using a SpectraMax microplate reader (Molecular Devices) at 544 nm excitation and 590 nm emission.[33]

Wound-Healing Assay

Cells were seeded with the same number in 6-well plates in complete medium. When the cells grew to 95% confluence, scratch wounds were created using 100-μL sterile pipette tips. To remove the suspended cells, the plates were washed with PBS twice. Images were captured in three defined fields at 0 and 48 hr, respectively.[34]

Matrigel Plug Angiogenesis Assay In Vivo

ECs were suspended in 400 μL of Matrigel, and, 48 hr later, the cells were imaged.

Statistical Analysis

Statistical analyses were performed with the SPSS 13.0 statistical package (SPSS). Multiple comparisons between groups were performed using ANOVA. Differences between the mean values were analyzed using Student's t test (parametric) and a Mann-Whitney U test (nonparametric). The data are expressed as the mean ± SE.

SUPPLEMENTAL INFORMATION

Supplemental Information includes seven figures and two tables and can be found with this article online at http://dx.doi.org/10.1016/j.ymthe.2017.03.031.

AUTHOR CONTRIBUTIONS

B.Z., W.-n.Y., X.-h.Z., Y.Z., L.-l.S., H.Z., and L.-s.J. carried out the experiments. B.Z., J.-k.W., T.S., and H.Z. reviewed the data and helped in the design and preparation of the manuscript.

ACKNOWLEDGMENTS

We thank Prof. Huajing Wan, Wuhan University, for gifting us the KLF5-flox mice. This study was supported by the National Basic Research Program of China (no. 2012CB518601), the National Natural Science Foundation of China (no. 31271396 and 31271224), Hebei Natural Science Foundation of China (no. H2016206406), the Fok Ying Tung Education Foundation (131037), and Hebei science and technology project (13967607D).

REFERENCES

1. Holmes, D. (2016). Cardiovascular endocrinology: Sugar drug reverses atherosclerosis. Nat. Rev. Endocrinol. *12*, 310.
2. Libby, P., Bornfeldt, K.E., and Tall, A.R. (2016). Atherosclerosis: Successes, surprises, and future challenges. Circ. Res. *118*, 531–534.
3. Shindo, T., Manabe, I., Fukushima, Y., Tobe, K., Aizawa, K., Miyamoto, S., Kawai-Kowase, K., Moriyama, N., Imai, Y., Kawakami, H., et al. (2002). Krüppel-like zinc-finger transcription factor KLF5/BTEB2 is a target for angiotensin II signaling and an essential regulator of cardiovascular remodeling. Nat. Med. *8*, 856–863.
4. Zhang, Y.N., Xie, B.D., Sun, L., Chen, W., Jiang, S.L., Liu, W., Bian, F., Tian, H., and Li, R.K. (2016). Phenotypic switching of vascular smooth muscle cells in the 'normal region' of aorta from atherosclerosis patients is regulated by miR-145. J. Cell. Mol. Med. *20*, 1049–1061.
5. Willeit, P., Skroblin, P., Kiechl, S., Fernández-Hernando, C., and Mayr, M. (2016). Liver microRNAs: Potential mediators and biomarkers for metabolic and cardiovascular disease? Eur. Heart J. *37*, 3260–3266.
6. Macias, S., Cordiner, R.A., Gautier, P., Plass, M., and Cáceres, J.F. (2015). DGCR8 acts as an adaptor for the exosome complex to degrade double-stranded structured RNAs. Mol. Cell *60*, 873–885.
7. Khan, M., Nickoloff, E., Abramova, T., Johnson, J., Verma, S.K., Krishnamurthy, P., Mackie, A.R., Vaughan, E., Garikipati, V.N., Benedict, C., et al. (2015). Embryonic stem cell-derived exosomes promote endogenous repair mechanisms and enhance cardiac function following myocardial infarction. Circ. Res. *117*, 52–64.
8. Fujiu, K., Manabe, I., Ishihara, A., Oishi, Y., Iwata, H., Nishimura, G., Shindo, T., Maemura, K., Kagechika, H., Shudo, K., and Nagai, R. (2005). Synthetic retinoid Am80 suppresses smooth muscle phenotypic modulation and in-stent neointima formation by inhibiting KLF5. Circ. Res. *97*, 1132–1141.
9. Nazari-Jahantigh, M., Wei, Y., Noels, H., Akhtar, S., Zhou, Z., Koenen, R.R., Heyll, K., Gremse, F., Kiessling, F., Grommes, J., et al. (2012). MicroRNA-155 promotes atherosclerosis by repressing Bcl6 in macrophages. J. Clin. Invest. *122*, 4190–4202.
10. Loyer, X., Vion, A.C., Tedgui, A., and Boulanger, C.M. (2014). Microvesicles as cell-cell messengers in cardiovascular diseases. Circ. Res. *114*, 345–353.
11. Deng, L., Blanco, F.J., Stevens, H., Lu, R., Caudrillier, A., McBride, M., McClure, J.D., Grant, J., Thomas, M., Frid, M., et al. (2015). MicroRNA-143 activation regulates smooth muscle and endothelial cell crosstalk in pulmonary arterial hypertension. Circ. Res. *117*, 870–883.
12. Zheng, B., Han, M., Shu, Y.N., Li, Y.J., Miao, S.B., Zhang, X.H., Shi, H.J., Zhang, T., and Wen, J.K. (2011). HDAC2 phosphorylation-dependent Klf5 deacetylation and RARα acetylation induced by RAR agonist switch the transcription regulatory programs of p21 in VSMCs. Cell Res. *21*, 1487–1508.
13. Hoshino, Y., Kurabayashi, M., Kanda, T., Hasegawa, A., Sakamoto, H., Okamoto, E., Kowase, K., Watanabe, N., Manabe, I., Suzuki, T., et al. (2000). Regulated expression of the BTEB2 transcription factor in vascular smooth muscle cells: Analysis of developmental and pathological expression profiles shows implications as a predictive factor for restenosis. Circulation *102*, 2528–2534.
14. Bafford, R., Sui, X.X., Wang, G., and Conte, M. (2006). Angiotensin II and tumor necrosis factor-alpha upregulate survivin and Kruppel-like factor 5 in smooth muscle cells: Potential relevance to vein graft hyperplasia. Surgery *140*, 289–296.
15. Ogata, T., Kurabayashi, M., Hoshino, Y., Ishikawa, S., Takeyoshi, I., Morishita, Y., and Nagai, R. (2000). Inducible expression of BTEB2, a member of the zinc-finger family of transcription factors, in cardiac allograft arteriosclerosis. Transplant. Proc. *32*, 2032–2033.
16. Demolli, S., Doebele, C., Doddaballapur, A., Lang, V., Fisslthaler, B., Chavakis, E., Vinciguerra, M., Sciacca, S., Henschler, R., Hecker, M., et al. (2015). MicroRNA-30 mediates anti-inflammatory effects of shear stress and KLF2 via repression of angiopoietin 2. J. Mol. Cell. Cardiol. *88*, 111–119.
17. Hergenreider, E., Heydt, S., Tréguer, K., Boettger, T., Horrevoets, A.J., Zeiher, A.M., Scheffer, M.P., Frangakis, A.S., Yin, X., Mayr, M., et al. (2012). Atheroprotective

communication between endothelial cells and smooth muscle cells through miRNAs. Nat. Cell Biol. *14*, 249–256.

18. Orekhov, A.N., Andreeva, E.R., and Bobryshev, Y.V. (2016). Cellular mechanisms of human atherosclerosis: Role of cell-to-cell communications in subendothelial cell functions. Tissue Cell *48*, 25–34.
19. Zhang, R.N., Zheng, B., Li, L.M., Zhang, J., Zhang, X.H., and Wen, J.K. (2014). Tongxinluo inhibits vascular inflammation and neointimal hyperplasia through blockade of the positive feedback loop between miR-155 and TNF-α. Am. J. Physiol. Heart Circ. Physiol. *307*, H552–H562.
20. Chattopadhyay, R., Dyukova, E., Singh, N.K., Ohba, M., Mobley, J.A., and Rao, G.N. (2014). Vascular endothelial tight junctions and barrier function are disrupted by 15(S)-hydroxyeicosatetraenoic acid partly via protein kinase C ε-mediated zona occludens-1 phosphorylation at threonine 770/772. J. Biol. Chem. *289*, 3148–3163.
21. Bazzoni, G., and Dejana, E. (2004). Endothelial cell-to-cell junctions: Molecular organization and role in vascular homeostasis. Physiol. Rev. *84*, 869–901.
22. Howe, G.A., and Addison, C.L. (2012). RhoB controls endothelial cell morphogenesis in part via negative regulation of RhoA. Vascular Cell *4*, 1.
23. Pankratz, F., Bemtgen, X., Zeiser, R., Leonhardt, F., Kreuzaler, S., Hilgendorf, I., Smolka, C., Helbing, T., Hoefer, I., Esser, J.S., et al. (2015). MicroRNA-155 exerts cell-specific antiangiogenic but proarteriogenic effects during adaptive neovascularization. Circulation *131*, 1575–1589.
24. Kundumani-Sridharan, V., Dyukova, E., Hansen, D.E., 3rd, and Rao, G.N. (2013). 12/15-Lipoxygenase mediates high-fat diet-induced endothelial tight junction disruption and monocyte transmigration: A new role for 15(S)-hydroxyeicosatetraenoic acid in endothelial cell dysfunction. J. Biol. Chem. *288*, 15830–15842.
25. Zhu, N., Zhang, D., Chen, S., Liu, X., Lin, L., Huang, X., Guo, Z., Liu, J., Wang, Y., Yuan, W., and Qin, Y. (2011). Endothelial enriched microRNAs regulate angiotensin II-induced endothelial inflammation and migration. Atherosclerosis *215*, 286–293.
26. Yang, Z., Zheng, B., Zhang, Y., He, M., Zhang, X.H., Ma, D., Zhang, R.N., Wu, X.L., and Wen, J.K. (2015). miR-155-dependent regulation of mammalian sterile 20-like kinase 2 (MST2) coordinates inflammation, oxidative stress and proliferation in vascular smooth muscle cells. Biochim. Biophys. Acta *1852*, 1477–1489.
27. Wang, C., Zhang, C., Liu, L., A, X., Chen, B., Li, Y., and Du, J. (2017). Macrophage-derived mir-155-containing exosomes suppress fibroblast proliferation and promote fibroblast inflammation during cardiac injury. Mol. Ther. *25*, 192–204.
28. Wan, H., Luo, F., Wert, S.E., Zhang, L., Xu, Y., Ikegami, M., Maeda, Y., Bell, S.M., and Whitsett, J.A. (2008). Kruppel-like factor 5 is required for perinatal lung morphogenesis and function. Development *135*, 2563–2572.
29. Zhou, W., Fong, M.Y., Min, Y., Somlo, G., Liu, L., Palomares, M.R., Yu, Y., Chow, A., O'Connor, S.T., Chin, A.R., et al. (2014). Cancer-secreted miR-105 destroys vascular endothelial barriers to promote metastasis. Cancer Cell *25*, 501–515.
30. Kessler, T., Zhang, L., Liu, Z., Yin, X., Huang, Y., Wang, Y., Fu, Y., Mayr, M., Ge, Q., Xu, Q., et al. (2015). ADAMTS-7 inhibits re-endothelialization of injured arteries and promotes vascular remodeling through cleavage of thrombospondin-1. Circulation *131*, 1191–1201.
31. Zhang, X.H., Zheng, B., Yang, Z., He, M., Yue, L.Y., Zhang, R.N., Zhang, M., Zhang, W., Zhang, X., and Wen, J.K. (2015). TMEM16A and myocardin form a positive feedback loop that is disrupted by KLF5 during Ang II-induced vascular remodeling. Hypertension *66*, 412–421.
32. He, M., Zheng, B., Zhang, Y., Zhang, X.H., Wang, C., Yang, Z., Sun, Y., Wu, X.L., and Wen, J.K. (2015). KLF4 mediates the link between TGF-β1-induced gene transcription and H3 acetylation in vascular smooth muscle cells. FASEB J. *29*, 4059–4070.
33. Lundeberg, E., Van Der Does, A.M., Kenne, E., Soehnlein, O., and Lindbom, L. (2015). Assessing large-vessel endothelial permeability using near-infrared fluorescence imaging–brief report. Arterioscler. Thromb. Vasc. Biol. *35*, 783–786.
34. Daniel, J.M., Prock, A., Dutzmann, J., Sonnenschein, K., Thum, T., Bauersachs, J., and Sedding, D.G. (2016). Regulator of G-protein signaling 5 prevents smooth muscle cell proliferation and attenuates neointima formation. Arterioscler. Thromb. Vasc. Biol. *36*, 317–327.

YMTHE, Volume *25*

Supplemental Information

Exosome-Mediated miR-155 Transfer from Smooth Muscle Cells to Endothelial Cells Induces Endothelial Injury and Promotes Atherosclerosis

Bin Zheng, Wei-na Yin, Toru Suzuki, Xin-hua Zhang, Yu Zhang, Li-li Song, Li-shuang Jin, Hong Zhan, Hong Zhang, Jin-shui Li, and Jin-kun Wen

Supplemental material

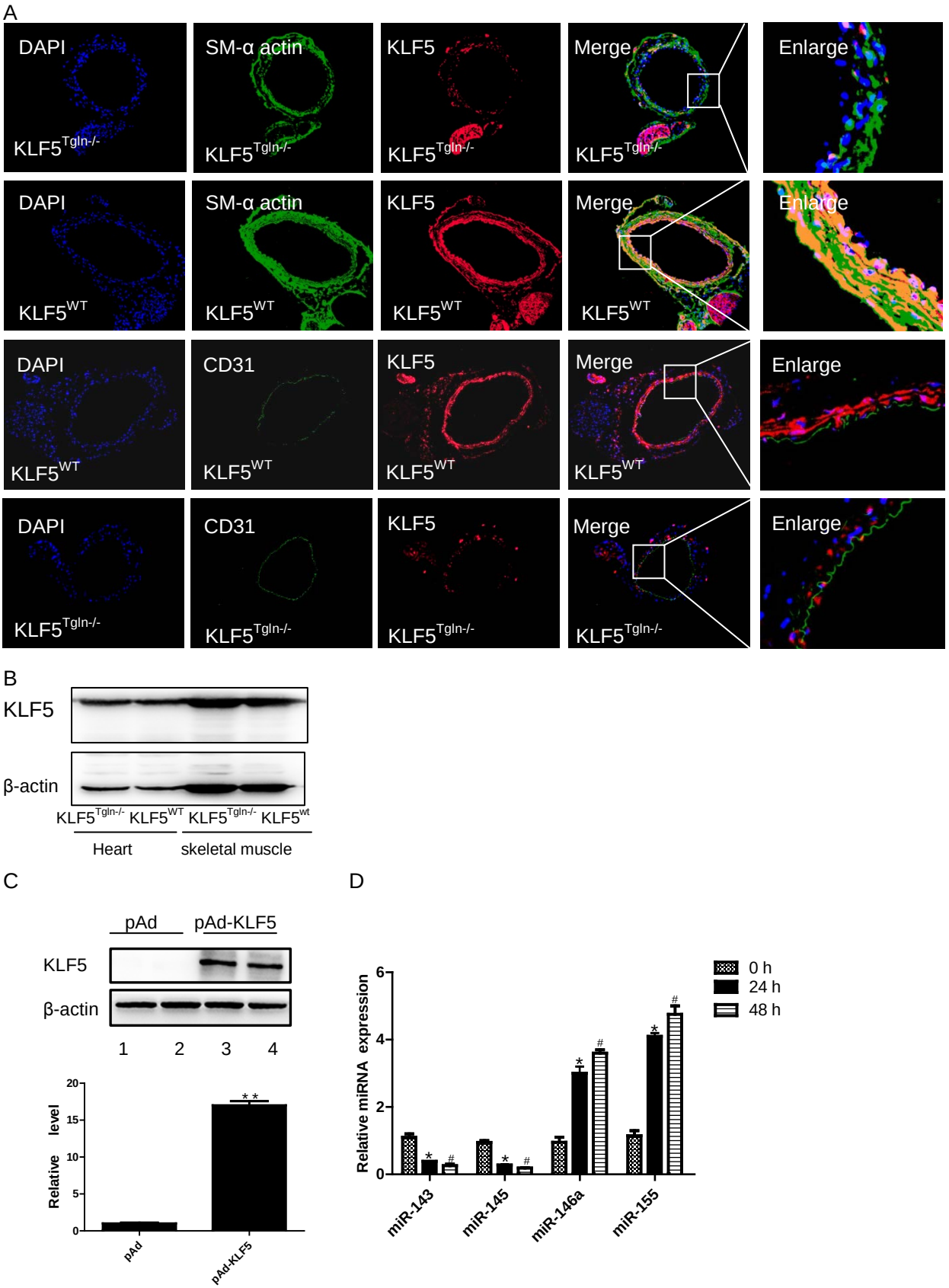

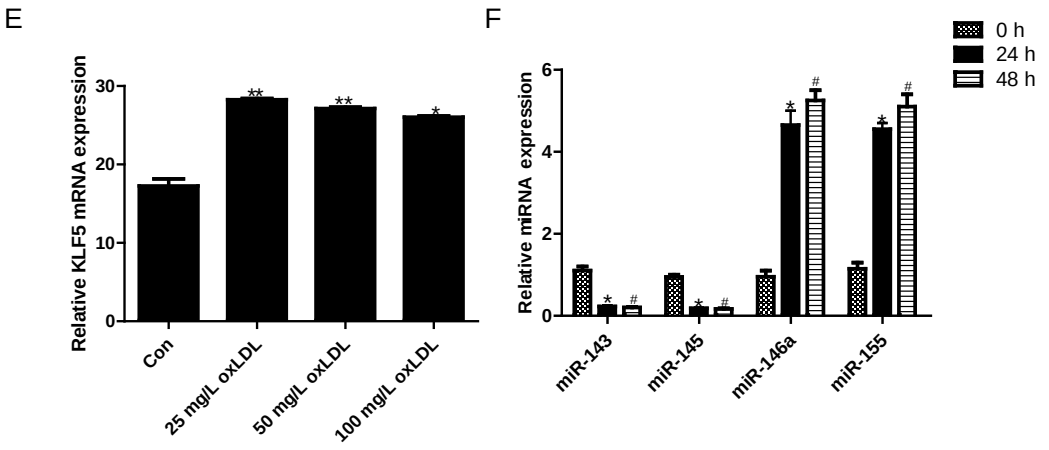

Figure 1. KLF5 regulates expression of miRNAs, particularly miR-155

A, Representative photographs of immunofluorescence staining with KLF5 staining, CD 31 and SM α-actin in carotid artery of $KLF5^{Tgln-/-}$ mice and $KLF5^{WT}$ mice. Magnification, ×100 (KLF5, SM α-actin staining and CD31 staining). B, KLF5 expression was detected by Western Blot (n=3) in different tissues of KLF5 in $KLF5^{Tgln-/-}$ (VSMC-specific knockout of KLF5) mice and $KLF5^{WT}$ mice. C, HASMCs were transfected with pAd or pAd-KLF5 for 48 h. KLF5 expression was detected by Western blotting (n=3). **P<0.01 vs pAd group. D, HASMCs were transfected with pAd or pAd-KLF5 for different times. miRNA expression was detected by real-time PCR (n=6). *P<0.05 vs 0 h group. $^{\#}$P<0.05 vs 0 h group. E, HASMCs were treated with oxLDL for 24 h. KLF5 mRNA expression was detected by Real-time PCR(n=6). *P<0.05 vs con group. **P<0.01 vs con group. F, HASMCs were treated with oxLDL for different times. miRNA expression was detected by real-time PCR (n=6). *P<0.05 vs 0 h group. $^{\#}$P<0.05 vs 0 h group.

Figure 2

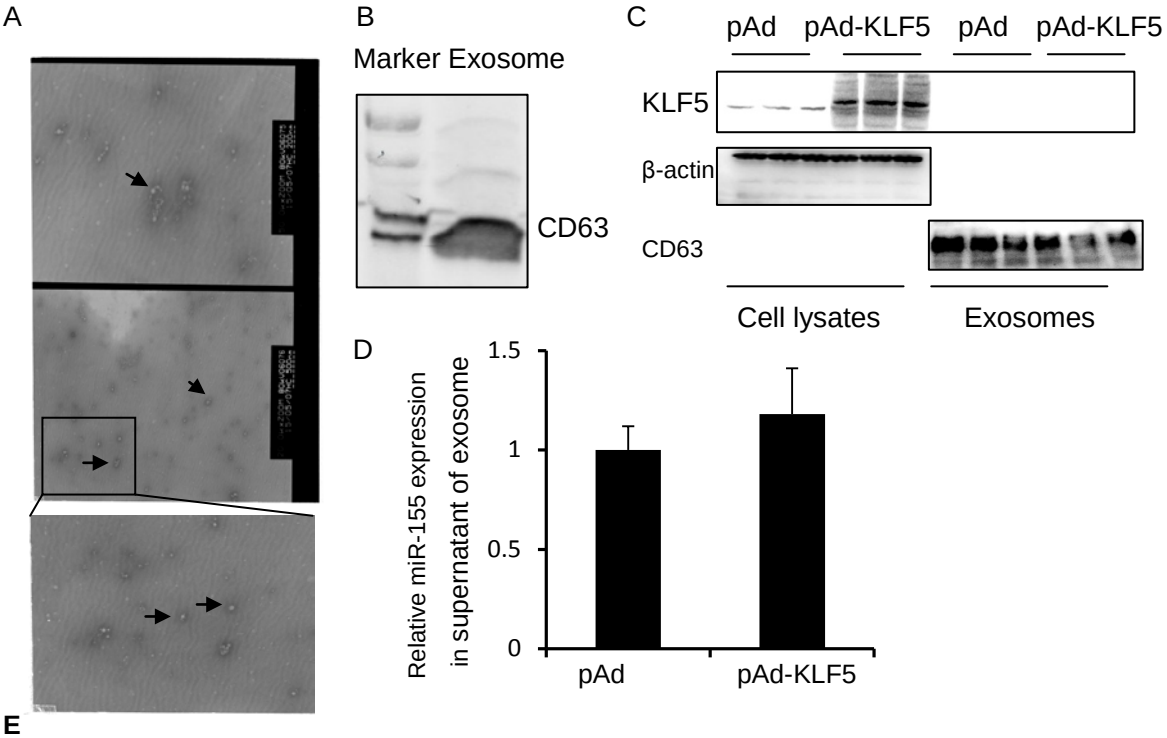

E

-1789agcaatttcctgtttctattaaagtgcattatacaaacttgtcattctggggatgaaaggt**caccc**tagaattgcctatgg
cgaac(mutated)
gcaatttcttatagttcaacctagaatgagaaatgggaaattcagaaaggcattgtaggcatctgtaaccagcagagggac
gtgccccacctgg**gtggg**gaccatgcatccttgccacatgccccactgcacaacttccccagctcctcaacgtca-1552
gcaag(mutated)

F

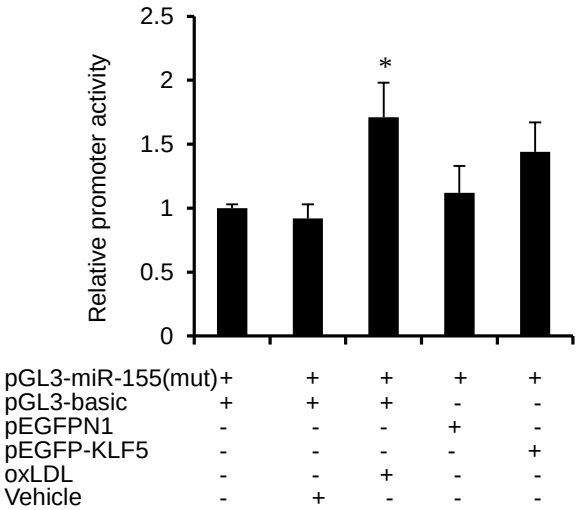

Figure 2. KLF5 induces enrichment of miR-155 in extracellular vesicles

A, Electron microscopy image of an isolated vesicle. B, Exosomes was extracted from the medium of VSMCs by ultracentrifuge. CD63 expression in exosomes was detected by Western Blotting (n=6). C, Exosomes were extracted from the medium of

VSMCs by ultracentrifuge. Cells were lysed and cell lysate was harvested. 20 μg protein was used to detected the expression of KLF5 and CD63 in exosomes by Western Blotting (n=3). D, miR-155 levels were detected by real-time PCR (n=6) in the remaining supernatant of exosomes from the medium of VSMCs. *P<0.05 vs pAd group. E, Part of ~2500 bp upstream sequence of pri-miR-155. KLF5 binding site was marked with underline (green). Mutated sites of KLF5 binding site was marked with underline (red). F, Reporter gene assay using miR-155 mutation promoter (n=6). VSMCs were transfected with indicated vectors for 48 h, luciferase activities were measured with the Dual-Luciferase Reporter System (Promega). Results are means±S.E.M. for six separate transfection assays with duplicate plates. *P <0.05 vs vehicle group.

Figure 3

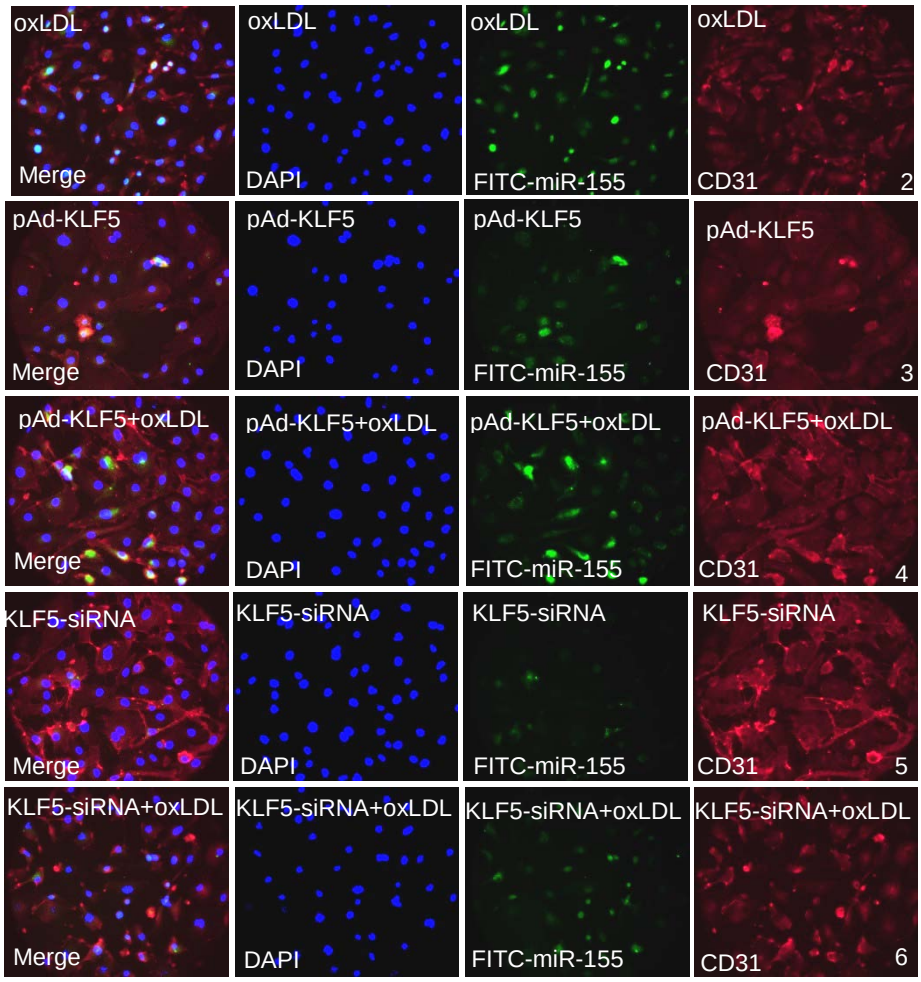

Figure 3 KLF5 affects the transmission of miR-155 between HASMCs and endothelial cells

An in vitro co-culture system was used where HASMCs are seeded in the top compartment, which is separated by a porous membrane from endothelial cells that are cultured in the bottom compartment. HASMCs (top compartment) were transfected with FITC-miR-155 together with indicated virus or siRNA and treated with or without oxLDL and co-cultured with endothelial cells (bottom compartment). FITC-miR-155 (green) and CD 31 expression (red) in endothelial cells was analyzed by confocal microscopy.

Figure 4

A

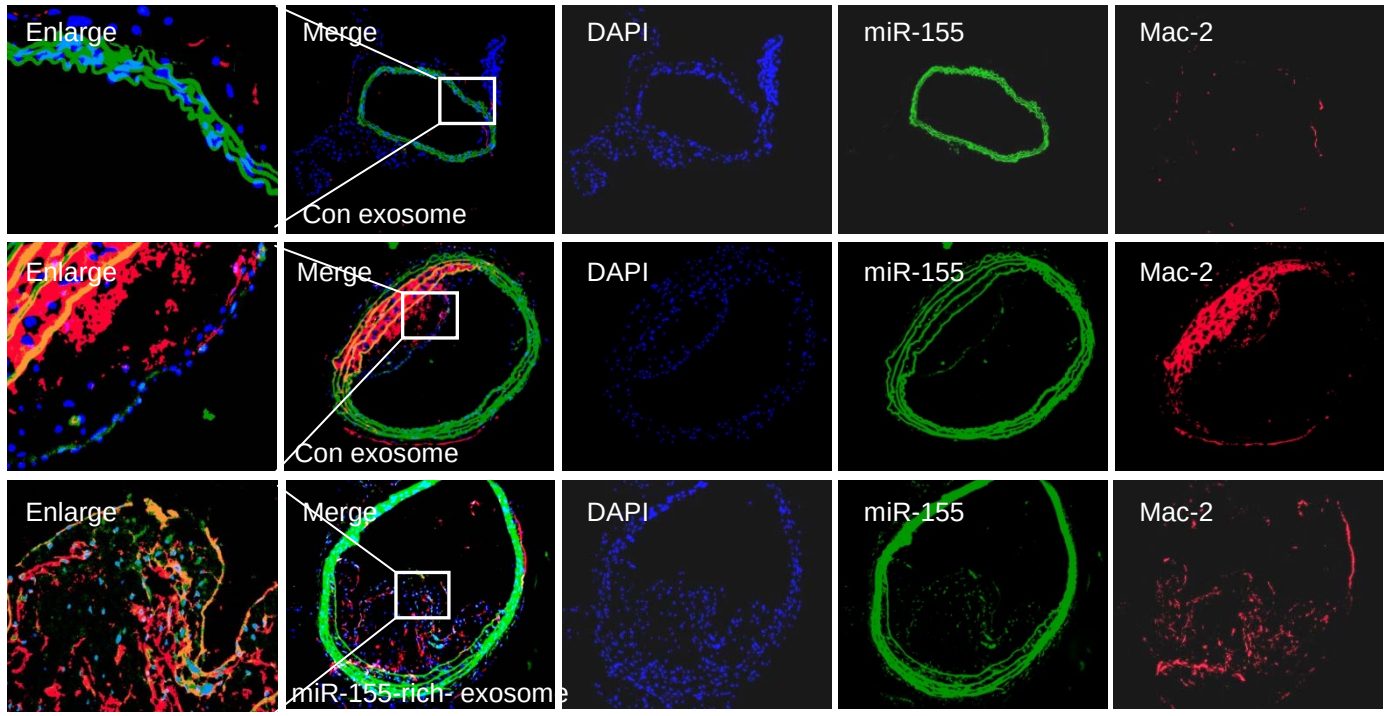
Normal feeding
HFD feeding
HFD feeding
Enlarge
Merge
DAPI
miR-155
Mac-2
Con exosome
miR-155-rich- exosome

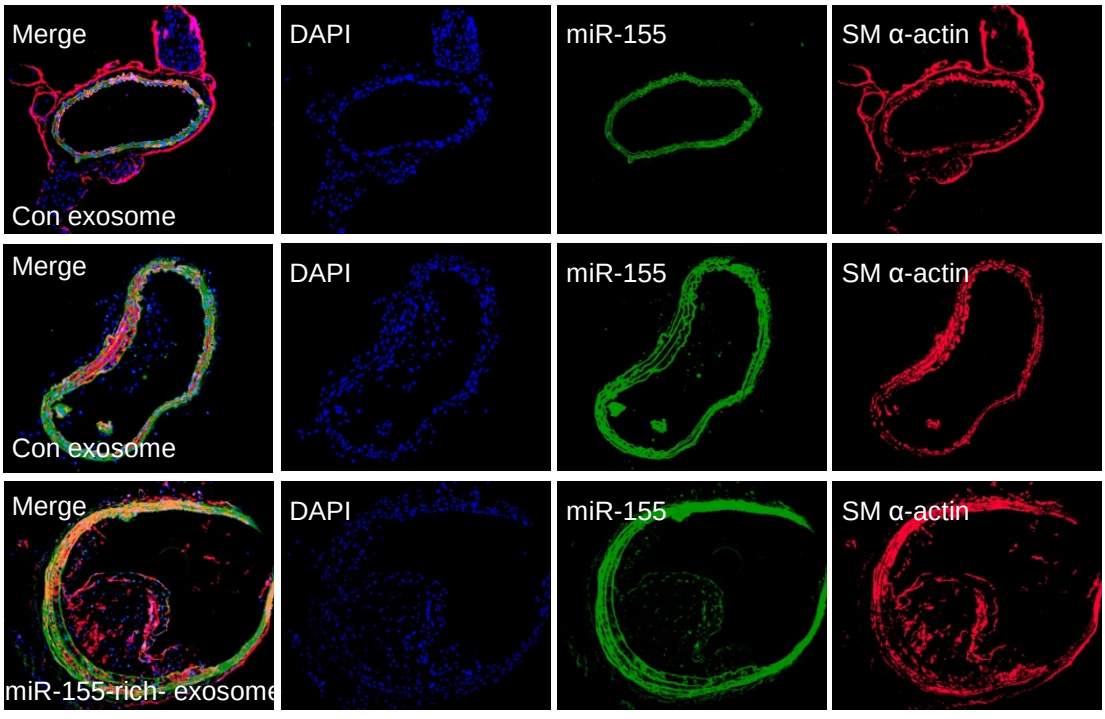
Normal feeding
HFD feeding
HFD feeding
Merge
DAPI
miR-155
SM α-actin
Con exosome
miR-155-rich- exosome

B

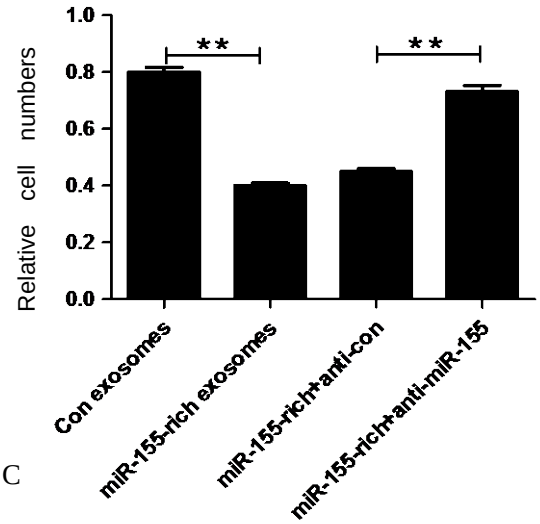
Relative cell numbers
1.0
0.8
0.6
0.4
0.2
0.0
**
**
Con exosomes
miR-155-rich exosomes
miR-155-rich+anti-con
miR-155-rich+anti-miR-155

C

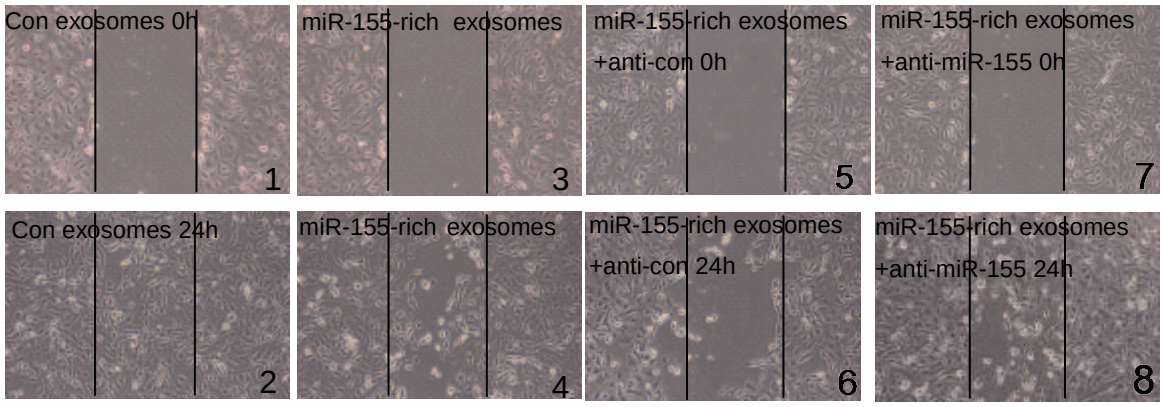
Con exosomes 0h
1
miR-155-rich exosomes
3
miR-155-rich exosomes
+anti-con 0h
5
miR-155-rich exosomes
+anti-miR-155 0h
7
Con exosomes 24h
2
miR-155-rich exosomes
4
miR-155-rich exosomes
+anti-con 24h
6
miR-155-rich exosomes
+anti-miR-155 24h
8

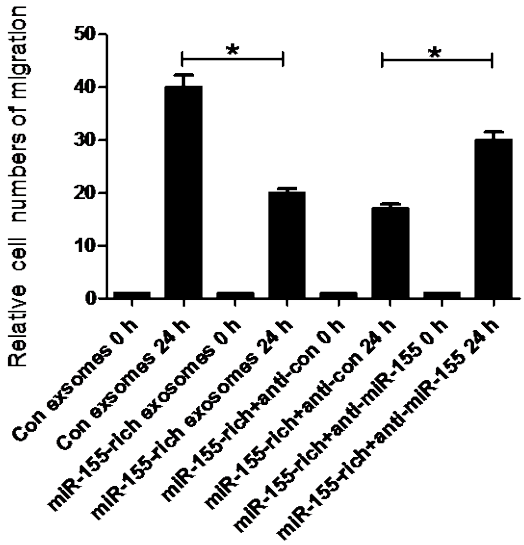
Relative cell numbers of migration
50
40
30
20
10
0
*
*
Con exsomes 0 h
Con exsomes 24 h
miR-155-rich exosomes 0 h
miR-155-rich exosomes 24 h
miR-155-rich+anti-con 0 h
miR-155-rich+anti-con 24 h
miR-155-rich+anti-miR-155 0 h
miR-155-rich+anti-miR-155 24 h

D

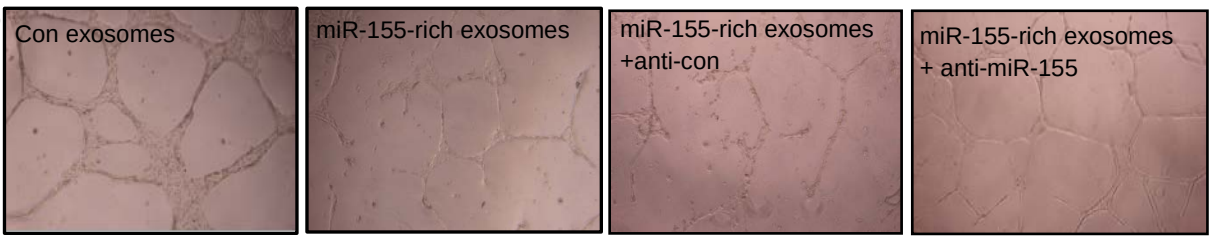
Con exosomes
miR-155-rich exosomes
miR-155-rich exosomes
+anti-con
miR-155-rich exosomes
+ anti-miR-155

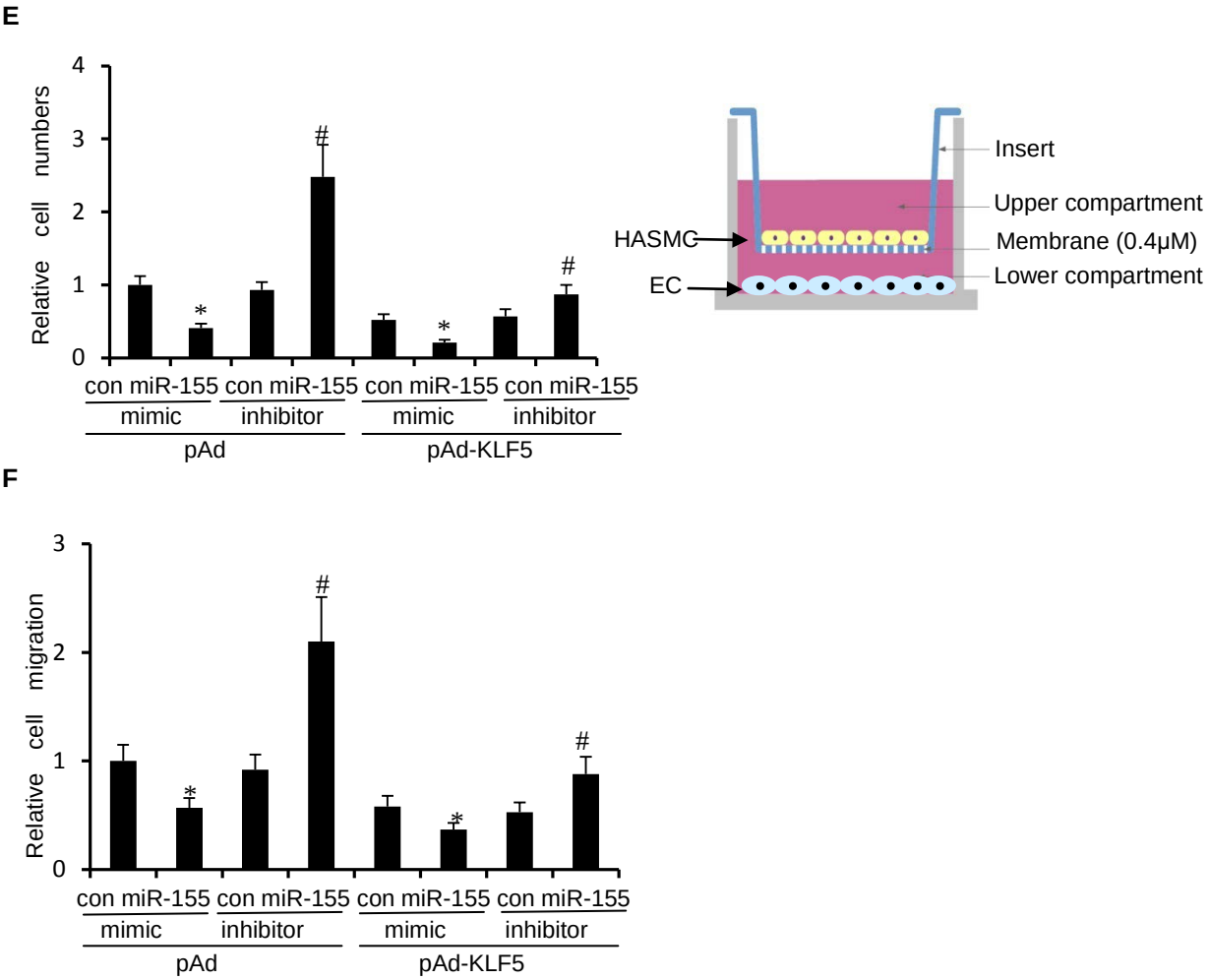

Figure 4. Vascular-derived miR-155 is transported to endothelial cells, leading to cellular dysfunction

A, Exosomes secreted by pAd- or pAd-KLF5-transduced HASMCs were intravenously injected into the tail vein of apoE$^{-/-}$ mice fed with HFD (n = 6) once a week. Representative photographs of miR-155 in situ hybridization (green) and mac-2 staining (red), SM α-actin staining (red), respectively. B, MTS assay was used to detect the proliferation of endothelial cells. **P <0.01 vs con exosome or miR-155-rich+anti-con group. C, Wound-healing assay was used to detect the migration of endothelial cells. *P <0.05 vs con exosome or miR-155-rich+anti-con group. D, Tube formation assay was used to detect the function of endothelial cells. E, An in vitro co-culture system was used where HASMCs were seeded in the top compartment, which is separated by a porous membrane from endothelial cells that are cultured in the bottom compartment. HASMCs (top compartment) were transfected with indicated mimic or inhibitor together with indicated virus and co-cultured with endothelial cells (bottom compartment). MTS assay was used to detect the proliferation of endothelial cells. *P <0.05 vs con mimic group or con mimic+pAd-KLF5 group, respectively. $^{\#}$P <0.05 vs anti-con group or anti-con+pAd-KLF5 group, respectively. F, Wound-healing assay was used to detect the migration of endothelial cells. *P <0.05 vs con mimic group or con

mimic+pAd-KLF5 group, respectively. $^{\#}P < 0.05$ vs anti-con group or anti-con+pAd-KLF5 group, respectively.

Figure 5

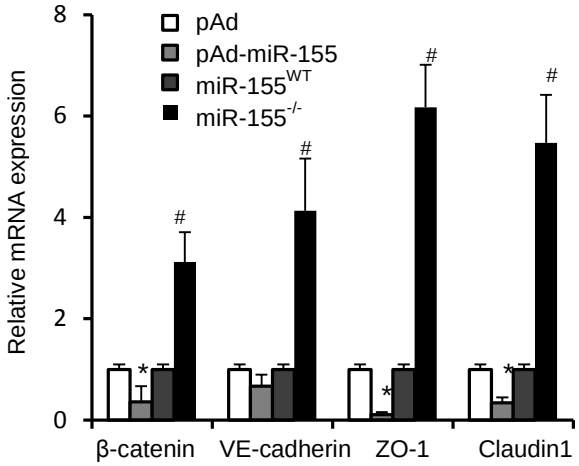

Figure 5. miR-155 regulates endothelial barrier function

pAd or pAd-KLF5 were intravenously injected into the tail vein of C57BL/6 mice (n = 6) once a week. Total miRNA from aortic tissue of miR-155^{WT} or miR-155$^{-/-}$ mice (n=6) were prepared and indicated TJ protein mRNA were detected by real-time PCR. *p< 0.05 vs pAd group; $^{\#}$p< 0.05 vs miR-155^{WT} group.

Figure 6

A

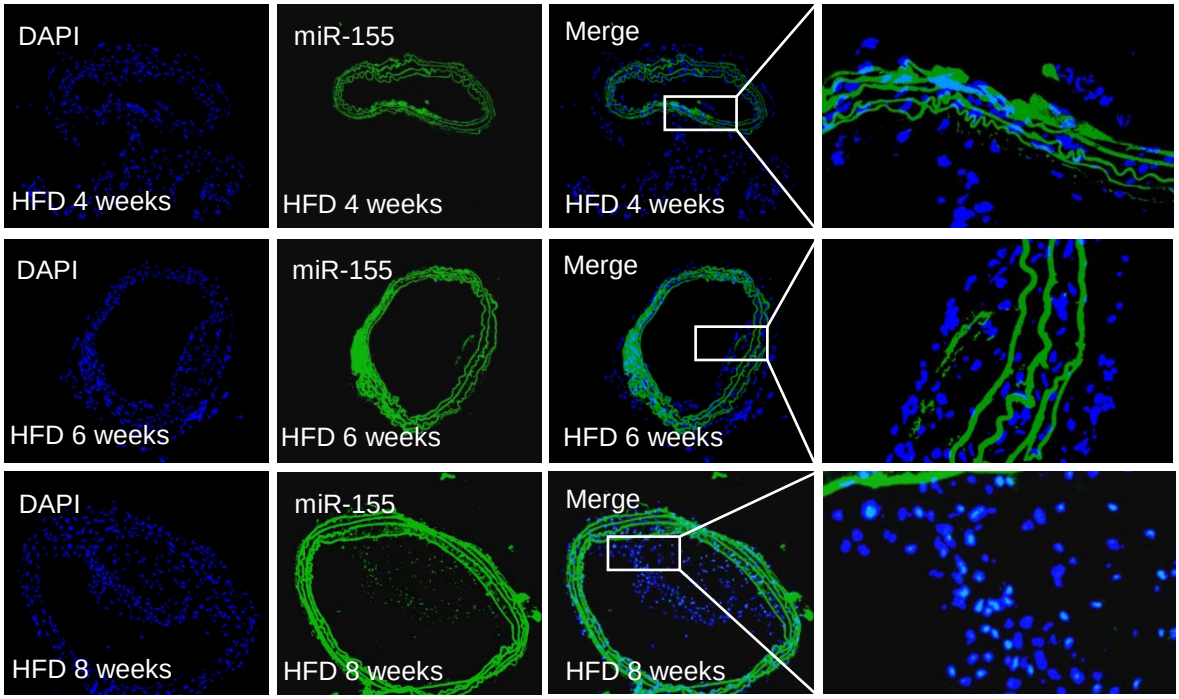
DAPI
HFD 4 weeks
miR-155
HFD 4 weeks
Merge
HFD 4 weeks
DAPI
HFD 6 weeks
miR-155
HFD 6 weeks
Merge
HFD 6 weeks
DAPI
HFD 8 weeks
miR-155
HFD 8 weeks
Merge
HFD 8 weeks

B

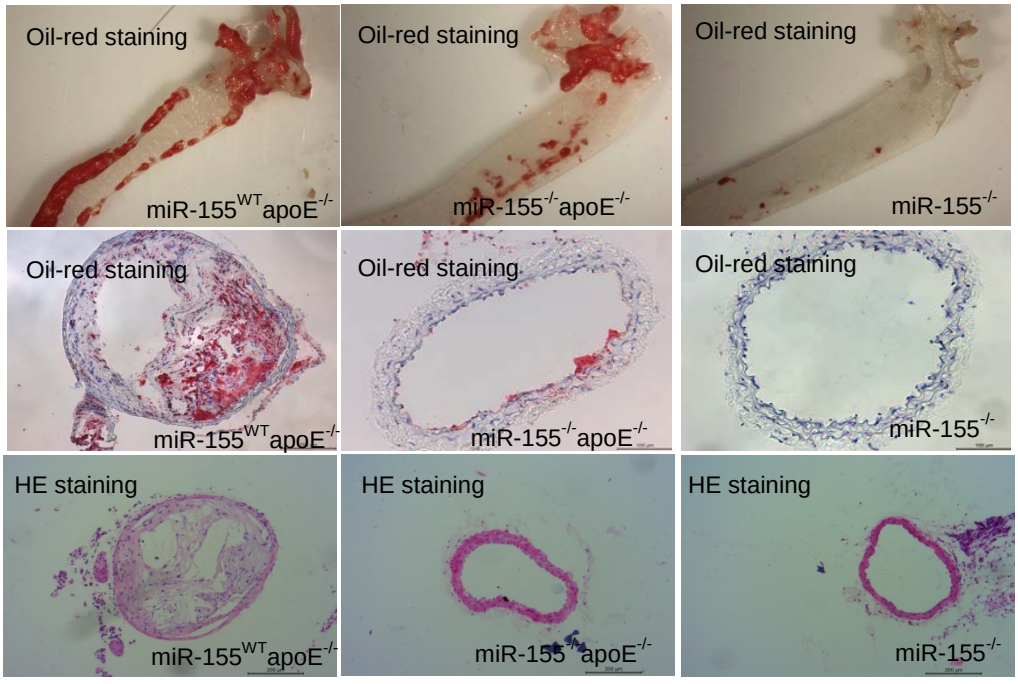
Oil-red staining
miR-155WTapoE-/-
Oil-red staining
miR-155-/-apoE-/-
Oil-red staining
miR-155-/-
Oil-red staining
miR-155WTapoE-/-
Oil-red staining
miR-155-/-apoE-/-
Oil-red staining
miR-155-/-
HE staining
miR-155WTapoE-/-
HE staining
miR-155-/-apoE-/-
HE staining
miR-155-/-

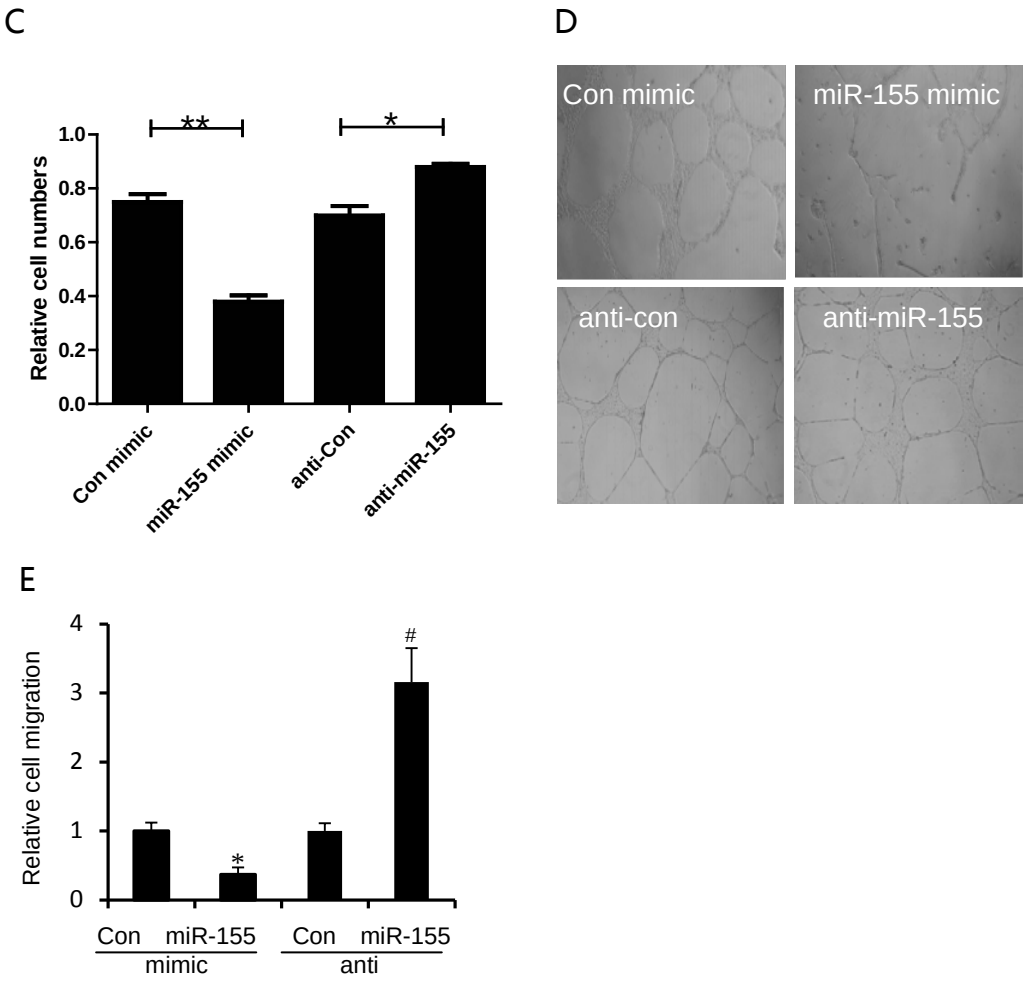

Figure 6. miR-155 inhibition suppresses atherogenesis

A, Representative photographs of staining of miR-155 by FISH in carotid artery of apoE$^{-/-}$ mice fed with HFD for 4 weeks, 6 weeks or 8 weeks, respectively. Magnification, ×100. B, Representative photographs of en face oil red O-stained thoracic aortas and HE-stained sections of the aortic root of apoE$^{-/-}$ or apoE$^{-/-}$miR-155$^{-/-}$ mice. C，Endothelial cells were transfected with miR-155 mimics or miR-155 inhibitor (anti-miR-155) for 24 h, and the proliferation of endothelial cells was then detected by MTS assay. **P<0.05 vs con mimic group. *P<0.05 vs anti-con group. D, Endothelial cells were transfected with miR-155 mimics or miR-155 inhibitor (anti-miR-155) for 24 h, and tube formation assay was performed. E, Endothelial cells were transfected with miR-155 mimics or miR-155 inhibitor (anti-miR-155) for 24 h, and the migration of endothelial cells was then detected by wound-healing assay. *P<0.05 vs con mimic group. $^{\#}$P<0.05 vs anti-con group.

Figure 7

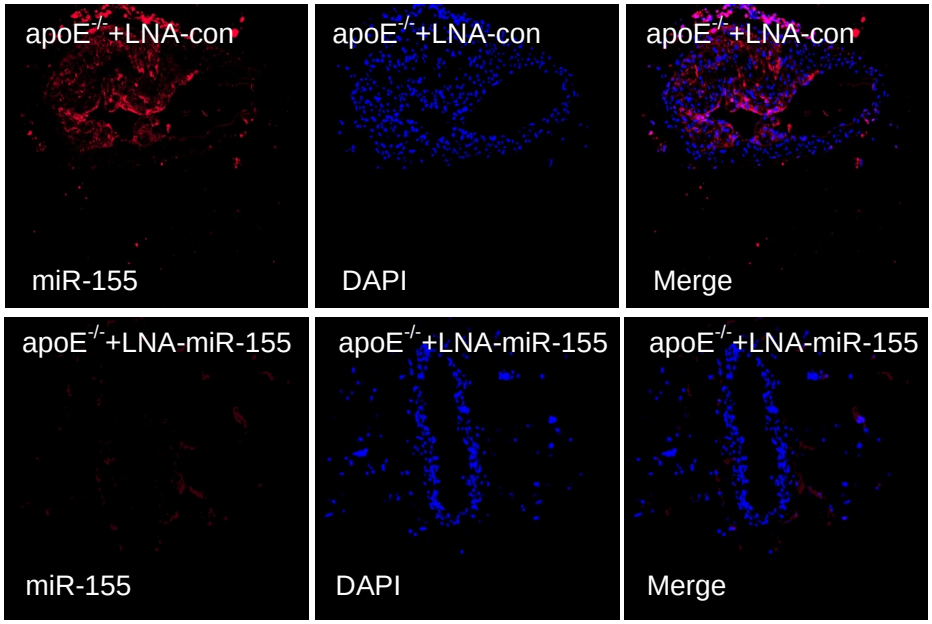

Figure 7 Inhibition of miR-155 prevents atherogenesis
Immunofluorence staining of miR-155(red) and DAPI (blue) in apoE$^{-/-}$ mice feed with HFD for 8 weeks.

Table I. miRNAs detected in HASMCs transfected with pAd or pAd-KLF5 displaying a variation lower than 2 between replicates

Upregulated miRNAs
hsa-miR-31-5p； hsa-miR-943； hsa-miR-24-3p； hsa-miR-625-5p； hsa-miR-4305； hsa-miR-3178； hsa-miR-1290； hsa-miR-4443； has-miR-29a-5p； hsa-miR-4290； hsa-miR-638； hsa-miR-20b-3p； hsv1-miR-H7-3p； hsa-miR-4791； hsa-miR-1304-5p； hsa-miR-935； hsa-miR-1285-3p； hsa-miR-4292； hsa-miR-421； hsa-miR-4449； hsa-miR-665； hsa-miR-1273e； hsa-miR-410-3p； hsa-miR-502-3p； hsa-miR-1469； hsa-miR-4732-5p； hsa-miR-1827； hsa-miR-1207-3p； hsa-miR-4644； ebv-miR-BART8-3p； hsa-miR-324-3p； hsa-miR-3195； hsa-miR-4530； hsa-miR-454-3p； hsa-miR-622； hsa-miR-493-3p； hsa-miR-4497； hsa-miR-652-3p； hsa-miR-214-3p； hsa-miR-199b-5p； hsa-miR-106a-5p； hsa-miR-4765； hsa-miR-1246；

Table II. miRNAs detected in HASMCs-derived exosomes transfected with pAd or pAd-KLF5 displaying a variation lower than 1.5 between replicates

Upregulated miRNAs
hsa-miR-381-3p； hsa-miR-4317； hsa-miRPlus-A1073； hsa-miR-26b-5p； hsa-miR-155-5p； hsa-miR-381-5p； hsa-miR-181d-5p； hsa-miR-154-3p； hsa-miR-190a-5p； hsa-miR-335-5p； hsa-miR-1185-1-3p； hsa-miR-320c； hsa-miR-885-5p； hsa-miR-376a-5p； hsa-miR-214-5p； hsa-miR-193a-3p； hsa-miR-543； hsa-miR-500a-5p/hsa-miR-500b-5p； hsa-miR-377-3p； hsa-miR-1207-3p； hsa-miR-26a-5p； hsa-miR-140-3p； hsa-miR-320a； hsa-miR-654-3p； hsa-miR-548t-5p； hsa-miR-5681b； hsv2-miR-H20； hsa-miR-34a-5p； hsa-miR-145-5p； hsa-miR-493-3p； hsa-miR-337-5p； hsa-miR-5571-5p； hsa-miR-432-5p； hsa-miR-143-3p； hsa-miR-154-5p； hsa-miR-551b-3p；